Profiling local translatomes and RNA binding proteins of somatosensory neurons reveals specializations of individual axons

Elizabeth S. Silagi[1,2], Ezechukwu Nduka[2], Maria F. Pazyra-Murphy[1,2], Jesus Zuniga Paiz[1,2], Shamsuddin A. Bhuiyan[1,3], Rosalind A. Segal[1,2,]*

[1]Department of Neurobiology, Harvard Medical School, Boston, MA, USA
[2]Department of Cancer Biology, Dana-Farber Cancer Institute, Boston, MA, USA
[3]Department of Neurology, Brigham and Women's Hospital
*Correspondence: Rosalind_segal@dfci.harvard.edu

SUMMARY

Individual neurons have one or more axons that often extend long distances and traverse multiple microenvironments. However, it is not known how the composition of individual axons is established or locally modulated to enable neuronal function and plasticity. Here, we use spatial translatomics to identify local axonal translatomes in anatomically and functionally specialized neurons in the dorsal root ganglia (DRG). DRG neurons extend long central and peripheral axons in opposite directions and distinct microenvironments to enable somatosensation. Using Translating Ribosome Affinity Purification and RNA sequencing, we generated a comprehensive resource of mRNAs preferentially translated within each axon. Locally translated proteins include pain receptors, ion channels, and translational machinery, which establish distinct electrophysiologic properties and regenerative capacities for each axon. We identify RNA-binding proteins associated with sorting and transporting functionally related mRNAs. These findings provide resources for addressing how axonal translation shapes the spatial organization of neurons and enables subcellular neuroplasticity.

HIGHLIGHTS

- Distinct mRNAs are localized to and translated in individual axons.
- Axonal translatomes govern regenerative capacity, translational machinery, and electrophysiology.
- The RBP, SFPQ, coordinates mRNA sorting towards peripheral somatosensory axons.
- Axonal translatome data can be explored at painseq.shinyapps.io/CompartmentTRAP/.

INTRODUCTION

Neurons possess several distinctive and essential features, including the ability to form long-range connections, efficiently propagate electrical signals, and exhibit plasticity in response to various stimuli. These capabilities rely on dynamic regulation of gene transcription and translation which together shape the cellular proteome. Transcriptional programs adapt rapidly to changes in the overall neuronal state, including alterations in membrane polarization, metabolic activity, and the inflammatory environment [1–3]. In contrast to transcription, translation can be regulated at the subcellular level, allowing for localized responses to changes in the microenvironment, such as those occurring at synapses and along the axons and dendrites [4–10]. As a result, local translation offers an additional layer of spatiotemporal regulation, fine-tuning the neuronal proteome in response to both global and microenvironmental signals.

It was not long ago that scientists believed local translation could not occur in axons. The first evidence of RNA in axons was detected in the 1960s [11,12], however, it took another 30 years of technological advances in microscopy for researchers to show that ribosomes were present in axons and capable of translating mRNA [13,14]. Since 2000, several studies have revealed that local protein synthesis is necessary for axon development and regeneration, and proteins transported from the soma are not sufficient to maintain local proteomes [5,15–17]. Despite this progress, it is not understood how mRNA transport and translation establish local proteomes and govern the specificity of axonal functions. Analysis of local translation in the axons of retinal ganglion cells in the central nervous system (CNS) suggests that translatomes are consistent across distinct axon branches [18]. However, this model does not answer whether local translation accounts for dynamic regulation of individual axonal proteomes.

In the peripheral nervous system (PNS), sensory neurons of the dorsal root ganglia (DRG), trigeminal ganglia, and nodose ganglia are distinguished by their pseudounipolar morphology, where a single axon stem bifurcates into central and peripheral projections that innervate the spinal cord and peripheral tissues, respectively [19,20]. In humans, each of these axons can extend up to 1 meter from the cell soma in the ganglion. The peripheral axons of DRG neurons are responsible for dynamically transducing environmental stimuli into electrical signals, while the central axons transmit these signals to the CNS. Both peripheral and central axons generate and propagate action potentials, are myelinated in many DRG subtypes, and exhibit the same microtubule orientation with plus-ends towards the terminals [20,21]. These spatially and functionally distinct central and peripheral axon branches make DRG neurons an ideal system for addressing how subcellular axonal translatomes differ and how any such differences contribute to the compartmentalized demands of encoding, transmitting, and filtering sensory information.

In this study, we generated a comprehensive resource to identify and compare the spatial translatomes of distinct somatosensory axons. The sodium channel Nav1.8 is expressed in approximately 60% of DRG neurons, including most subtypes involved in pain sensation [19,22,23]. Using Nav1.8^{cre}; L10a-GFP$^{fl/fl}$ mice and a combination of Translating Ribosome Affinity Purification and highly sensitive RNA sequencing (TRAP-Seq) [24], we profile the central and peripheral axonal translatomes of somatosensory neurons from microdissected mouse tissues—specifically, 1) lumbar DRG cell bodies, 2) sciatic nerves (peripheral axons), and 3) lumbar dorsal roots (central axons). Our analysis identifies hundreds of axon-selective transcripts, including specialized ion channel isoforms with preferential translation in either central or peripheral axons. These findings indicate that translation is an indispensable mechanism for locally modulating axonal physiology within distinct branches of the same neuron. Furthermore, we show that many of the locally translated mRNAs are selectively targeted to the central versus peripheral axons, indicating that there is disparate transport and/or stabilization of individual mRNAs in these two axon branches. Notably, SFPQ, an RNA-binding protein (RBP) implicated in axonal transport of RNA regulons[25], is preferentially expressed in peripheral axons and predominantly binds to mRNAs that are translated in these peripheral branches, suggesting that SFPQ and other RBPs enable selective localization of functional RNAs cargoes to individual axons. Together, our findings offer a comprehensive understanding of how local translation contributes to the spatial organization of neuronal function. This resource (http://painseq.shinyapps.io/CompartmentTRAP) provides a wealth of data to investigate how cellular functions are selectively regulated at the local level and highlights how dysregulation of axonal translatomes may contribute to neurodegenerative diseases and disorders.

RESULTS

Defining subcellular translatomes in somatosensory dorsal root ganglia neurons

To generate a comprehensive resource of the axonally transported and translated mRNAs in dorsal root ganglia (DRG) sensory neurons *in vivo*, we performed spatial translatomics using Translating Ribosome Affinity Purification (TRAP) paired with ultra-low methods for RNA-sequencing to account for technical difficulties of extracting high-integrity RNA from axons *in vivo*. The lumbar ganglia (soma), sciatic nerves (peripheral axons), and lumbar dorsal roots and spinal cords (central axons) were microdissected from ~15 perinatal mice (week 1) containing GFP-tagged ribosomal subunits in Nav1.8+ neuronal cell types (Nav1.8^{cre};L10a-GFP$^{fl/fl}$) (Fig. S1A). Ribosome-associated mRNAs were isolated from tissue lysates using GFP-antibody affinity purification and ultra-low concentration RNA extraction yielding ~10-100 pg/µL RNA (Fig. S1B,C). We carried out the same procedure on littermate negative control mice (L10a-GFP$^{fl/fl}$) that lacked GFP-tagged ribosomes. Libraries were prepared from low input total RNA samples with SMART-Seq, and subsequently sequenced and aligned to elucidate the distinct central and peripheral axonal translatomes (n=4 sets/condition, each set consisted of 13-17 individual animals) (Fig. S1D) [26].

Principal component analysis and pair-wise comparisons demonstrate that the DRG soma samples cluster together across the multiple samples, while central and peripheral axon samples cluster distinctly from the soma and from each other (Fig. 1A). This distinct clustering indicates that although the DRG axons yield low abundance RNA, the transcripts were highly specific for each compartment. Overall, we detected active translation of 12,207 transcripts in the DRG soma compartment, while local translation of 9789 and 1477 transcripts were detected in the sciatic nerve and lumbar dorsal root/spinal cord fractions,

respectively (Fig. 1B, Table S1-3). The majority of RNAs translated in the bulk sciatic nerve, dorsal root, and spinal cord tissues are not derived from Nav1.8+ sensory axons, but rather from local glia, epineural cells, and neuronal cell bodies in the spinal cord. To distinguish which of the thousands of transcripts were definitively derived from Nav1.8+ sensory neurons, rather than non-neuronal and non-specific transcripts, we determined the transcripts with significantly higher expression in Nav1.8-GFP samples as compared to negative controls lacking L10a-GFP (p.adj ≤ 0.05) (Fig. 1C-E) [27]. After bioinformatically filtering out the background transcripts with high expression in negative controls, the specific translatomic gene lists were refined to include 549 transcripts from the soma, 304 from the peripheral axons, and 225 from the central axons- with very few transcripts shared (p.adj ≤ 0.05) (Fig. 1F, Table S4-6). Using this method of stringent background filtering, we established high confidence cohorts of locally translated mRNAs within DRG soma and peripheral and central axons. However, we cannot conclude that mRNAs absent from the gene lists are *not* locally translated, as they may have been filtered out through the strict confidence interval of our bioinformatic approach.

The dorsal root ganglia (somatic compartment) are the hub for mRNA transcriptional and translational machinery for all DRG neurons. The mRNAs translated within the DRG soma encoded proteins related to fundamental gene ontological (GO) biological processes such as proteasomal catabolism, protein complex assembly, and microtubule cytoskeletal organization (Fig. 2A,B; Table S7) [28,29]. Only 16.5% of these transcripts were also clearly translated in axons: 30 transcripts were shared with peripheral axons and 61 with central axons (Table S8). These shared transcripts largely encoded membrane proteins (GO Cellular Component: Membrane; p.adj: <0.0063), cilium/flagellum proteins (GO Cellular Component: Cilium; p.adj: <0.022), and lysosomal proteins (GO Cellular Component: Lysosome; p.adj: <0.0022). Conversely, the background transcripts filtered out of the somatic gene list were associated with glial function, extracellular matrix organization, and broad developmental processes (Fig. 2C,D). This confirms that bioinformatic background filtering effectively removed non-neuronal transcripts from our compartmentalized datasets.

Central and peripheral DRG axons have distinct translatomes

The background-filtered axonal translatomes show a remarkable heterogeneity. First, there are two sets of axonally translated mRNAs: 1) those translated only in axons, implying autonomous control over protein availability, and 2) those translated in both axons and soma, implying protein transport from the soma can also contribute to axonal protein availability (Table S8). Interestingly, most transcripts were axon-specific, highlighting the significance of subcellular translational control; ~80% of the transcripts were unique to axons, while only 20% were translated in the soma as well. Furthermore, the two axonal translatomes were highly distinctive from one another and expressed transcripts directly related to their unique subcellular function. Only 13 transcripts were shared between peripheral and central axons, 7 of which were also found in the soma translatome (Table S8). The most relevant of the genes shared between the two axons, but not expressed in the soma encode for potassium ion channels (*Kcnk12/ Kcnmb1*) and the neuropeptide Y receptor (*Npy2r*). The local translation of these components may enable rapid modification in the electrophysiology of pain transmission. However, the most notable discoveries about the axonal translatomes are not their similarities but rather how they diverge. Most locally translated mRNAs were only detected in either the central or peripheral axon. The individual mRNAs identified are quite different in the two axon branches. However, GO functional enrichment analysis performed on the refined gene lists for these two distinct translatomes revealed that many of the components translated in axons overall are involved in neuronal firing, nociceptive processing, regenerative capacity, and translational machinery (Table S9,10).

The 304 locally translated mRNAs in the peripheral axon were enriched for transcripts encoding proteins related to synaptic organization, axon terminus formation, ciliary basal bodies, and ribosomal maintenance (Fig. 3A,B). We applied a gene concept network to display the genes associated with the enriched GO terms (Fig. 3C). Notably, numerous neurotransmitter receptors (*Gabrb3, Grin2a, Adra2c, Adgra1*) and ion channels (*Hcn1, Scn2a*) are locally translated in peripheral axons. These components enable peripheral synaptic specialization and action potential propagation. Changes in *Grin2a* mRNA stability and translation have been implicated in neuropathic pain [30], while *Hcn1* encodes a hyperpolarization activated cyclic nucleotide gated channel protein that is involved in transmitting nociceptive signals and is overexpressed in many neuropathic pain syndromes [31]. We also identified

transcripts encoding the calcium channel, Catsper*2*, which was initially identified as a voltage-dependent, Ca^{2+} selective, pH-sensitive ion channel highly expressed in sperm, as well as two ancillary components of this channel (Catsperd and Catsperζ) [32]. Thus, several components that are locally translated in the peripheral axons play critical roles in membrane physiology and nociception and indicate that regulated axonal translation may modify pain responses.

Further analysis of the datasets demonstrates that several proteins involved in ciliary basal bodies (*Pifo, Lca5, Odf2l*) are also locally translated in the peripheral axons. Ciliary proteins function in cytoskeletal organization and transport [33], and so the local translation and production of these components may provide peripheral axons with the ability for axonal growth and repair, an ability that is not shared with the central axons [21]. Finally, we identified several locally translated ribosomal subunits in the peripheral (but not central) axons, including intermediate/surface-depth 40s, 60s, and ribosomal-ubiquitin fusion proteins (*Rpl7, Rps15a, Rps27a, Rps30/Fau*) (Fig. S2A,B) [34]. These findings are consistent with previous studies demonstrating the importance of newly translated ribosome proteins in remodeling and maintaining the translational machinery needed for local protein synthesis [35]. Two of the locally translated mRNAs, *Rps15a* and *Rps30/Fau*, contain a CUIC sequence motif within their transcripts. This motif has been shown to control axonal translation of ribosomal proteins through an RNA-loop structure immediately upstream of the translation initiation codon [36]. These findings highlight the importance of autonomous ribosomal adaption and repair within the long axons of the peripheral nervous system and suggest that locally translated ribosome may contribute to the regenerative capacity of such axons.

The 225 mRNAs locally translated in the central axons were largely distinct from those identified in the peripheral axons. The central axon translatome was enriched for transcripts required for serotonin binding, sensory perception of pain, and sensory perception of external/temperature stimulus (Fig. 4A,B). Local translation of serotonin receptors, *Htr3a* and *Htr5a,* in the central axons suggest serotonin binding may be an important component of descending modulation of nociceptive inputs from primary somatosensory neurons (Fig. 4C). This finding expands the current view of descending serotonergic pain modulation, which has been thought to involve binding to 5-HTR3A (encoded by *Htr3a*) on inhibitory spinal cord interneurons [37,38]. Multiple distinct serotonin receptors were also identified in the somatic datasets, including *Htr1a* and *Htr5a* (Table S4). While Htr3a encodes a receptor that functions as a ligand-gated ion channel, Htr1a and Htr5a encode G-protein coupled receptors [39]. These data suggest that different areas of the cell can respond to serotonin but may do so via distinct receptor classes that have drastically different implications for cellular physiology. Several genes encoding ion channel proteins were also identified in this central axon gene set, including *Scn11a,* which encodes Nav1.9. The sodium channel Nav1.9 is selectively expressed in DRG neurons and point mutations in this channel protein can cause either hyperexcitability and chronic pain or chronic insensitivity to pain [40]. Thus, several receptors and channels identified in the central axon dataset are distinct from those identified in peripheral axons.

We also found evidence for local translation of additional key somatosensory receptors, including *Trpv1, Ntrk1, and Asic3,* which are implicated in peripheral sensory detection and signal integration (Fig. 4C) [41,42]. In addition, *Calca,* which encodes CGRP, is present in the central axon dataset. The CGRP neuropeptide is released both by the central and peripheral axons of DRG neurons, and this neuromodulator is critical for pain signaling throughout the body [43]. Expression and release of CGRP are regulated transcriptionally; our data suggest that local regulation of *Calca* translation may also impact pain signaling and the transmission of nociceptive responses to the CNS. It is important to note that while we found that *Calca, Trpv1,* and other nociceptive receptors are locally translated in the central axon compartment which included central axon terminals, it is possible that these may also be translated in peripheral axon terminals in the skin, which were not sampled in our peripheral translatome from the sciatic nerve.

DRG axons locally translate specialized ion channels and membrane-bound receptors

Surprisingly, the axonally translated mRNAs in both the central and peripheral axons encode a significant number of membrane-embedded receptors and channels, such as voltage-gated ion channels, neurotransmitter receptors, and somatosensory receptors. Translation of these proteins within axons requires both an active signal recognition particle to link the newly translated protein to a membrane, and the glycosylation machinery that is normally located in the Golgi Apparatus [16,44]. The association of these

mRNAs with ribosomes containing L10a-GFP as shown in the TRAP experiments provide clear evidence that these mRNAs are likely to be translated into protein in the central or the peripheral axons, despite the complexity of producing membrane-embedded components.

To verify our findings of local and selective translation in the central or peripheral axons, we focused on several of the channels and receptors identified in our screen. Puromycin was intraperitoneally injected into mice for 20 minutes to label nascent protein chains in the dorsal root ganglia, sciatic nerves, and dorsal roots (Fig. 5A). Proximity labeling (Puro-PLA) enabled the visualization of specific nascent proteins via proximity of antibodies bound to puromycin and the translating protein of interest (Fig. S3). To make sure that we are analyzing nascent peptides within the axons correlating to our TRAP experiments, we focused on PLA puncta that are within the Nav1.8 labeled axons. PLA visualization and quantification verify that individual mRNAs identified by TRAP-Seq as being preferentially translated in the peripheral axons of the sciatic nerve (*Hcn1* and *Scn2a*) are indeed translated there, and that we find very little translation in the central axons of the dorsal roots (Fig. 5B-C''). In contrast, our analysis indicates that there is extensive translation of *Htr3a* and *Scn11a* in central axons, with little or no translation taking place in the peripheral axons (Fig. 5D-E''). These findings validate our TRAP-Seq results and indicate that the data in these translatomes provide a useful resource for identifying components that are locally translated. Moreover, we can conclude that there is localized synthesis of specific ion channels in each axon which may contribute to the function and identity of peripheral and central axons.

mRNAs encoding locally translated proteins are selectively targeted to axons

For the identified proteins to be translated in either axon, the corresponding mRNA must both be transported to the axon and engage with translational machinery at that location. To determine whether the distinct translatomes of the central and peripheral axon reflect differential localization of the mRNA transcripts, or whether these mRNAs are similarly localized to both axons but are selectively translated at one site, we utilized *in vivo* RNAscope fluorescent *in situ* hybridization (FISH) to evaluate the subcellular localization of select mRNAs. Single molecule RNAscope demonstrated the mRNA expression pattern for mRNAs encoding *Hcn1, Scn2a, Htr3a, Scn11a, Catsper2*, and *Trpv1* within the DRG soma, sciatic nerves (peripheral), and dorsal roots (central) (Fig. 6A-D', Fig. S4). Again, we focused on RNAscope puncta that are within the Nav1.8 labeled axons, or within the Nav1.8 cell bodies in the DRGs. Using particle analysis, we found that *Hcn1, Scn2a,* and *Catsper2* transcripts have significantly more puncta per area in Nav1.8+ peripheral axons compared to central axons, indicating that these transcripts are both selectively localized and selectively translated in peripheral axons (Fig. 6A-B', E, F; S4A-B'). In contrast, *Htr3a* and *Scn11a* have significantly more puncta per area in Nav1.8+ central axons than in peripheral axons (Fig. 6C-D', G, H). As expected, these mRNAs were all also localized to the Nav1.8+ cell bodies of DRG neurons. Notably, *Trpv1* mRNA, which was identified in our translatome as being translated in the central axon, is present in both central and peripheral axons *in vivo* (Fig. S4C,C'). This suggests that there may either be differential modulation of TRPV1 translation in the two axons, or that TRPV1 is largely translated at axon terminals which we know were included in the central but not peripheral axon tissue collection. These data indicate that the distinct axonal translatomes in the central and peripheral axons predominantly reflect differential transport and localization of the mRNAs from the cell body to one axon or the other.

RBPs are positioned to orchestrate the subcellular localization of axonal translatomes

Our PLA and RNAscope findings indicate that many of the channels and receptors critical for initiating and propagating somatosensation are locally produced within either the central or peripheral axon, and that the corresponding mRNAs are highly localized to one or the other axon as well (Table S11). An important step in enabling such highly localized and regulated translation is the sorting and transport of mRNAs to distinct subcellular regions. Sorting of mRNAs to specific locations often depends on structural elements within mRNA sequences; axonal mRNA sorting is usually coordinated through RNA binding protein (RBP) recognition of select localization motifs within the 3' untranslated region (3'UTR) of the target mRNA [45]. RBP-bound mRNAs assemble into ribonucleoprotein (RNP) transport granules, characterized by their ability to undergo liquid-liquid phase separation and be transported directly or indirectly along microtubules by motor proteins [46–48].

To investigate the potential logic for differential RNA sorting to central and peripheral axons, we bioinformatically analyzed the 3'UTRs of axonally translated mRNAs, with the goal of identifying RBPs that selectively bind and traffic mRNAs to one or the other axon [45]. RBPs were identified as candidates for mRNA sorting if they fulfilled two criteria: 1) multiple binding motifs for that RPB are in the 3'UTR of key axonally translated mRNAs and 2) the RBP is predicted and/or demonstrated to undergo phase separation and be present in RNA granules [46–48]. A heatmap displaying the number of individual motifs per 3'UTR was used to rank RBPs that were significantly more associated with peripherally or centrally translated mRNAs (Fig. S5A). We determined that 16 RBPs similarly bound the 3'UTRs of peripherally and centrally translated mRNAs, 84 RBPs had more binding sites within peripherally translated mRNA transcripts, and 24 RBPs had more binding sites within centrally translated mRNA transcripts (Fig. S5A).

We further investigated the three cohorts of RBPs using the STRING database protein-protein interaction functional annotation analysis (Fig. S5B-D) [49]. As predicted, all cohorts were enriched for RBPs involved in RNP granules cellular components. The set of RBPs that are predicted to bind equally to mRNAs present in the peripheral and central axons were enriched for nuclear proteins (Fig. S5B). RBPs predicted to bind to the centrally located and centrally translated mRNA were enriched for cytoplasmic proteins that are involved in both RNP and stress granules, rather than nuclear proteins (Fig. S5C). Interestingly, peripheral-associated RBPs were instead enriched for proteins with specific neuronal functions in the synapse, dendrite, and distal axon (Fig. S5D). These data prompted us to examine the possibility that some of these RBPs may be constituents of cytoplasmic RNP granules involved in axonal transport and translation.

If individual RBPs are implicated in mRNA sorting and axon-specific translation, we would expect to see spatially selective expression of these RBPs in the axons *in vivo*. Therefore, several candidate RBPs were further investigated to determine if *in vivo* axonal localization patterns correlate with their predicted mRNA binding patterns. We focused on the localization patterns of Splicing factor proline- and glutamine-rich (SFPQ), Fus-interacting protein 1/ serine and arginine rich splicing factor 10 (Fusip1/SRSF10), and Embryonic lethal, abnormal vision, drosophila-like 1 (HuR/ELAVL1). Interestingly, SFPQ contains 3'UTR binding sites on multiple peripherally translated mRNAs required for axonal and synaptic function including *Hcn1, Gabrb3, Calb1,* and *Dnajc6* (Fig. S5A). In contrast, SRSF10 contains 3'UTR binding sites on multiple centrally translated mRNAs encoding ion channels and receptors related to pain signaling: *Htr3a, Htr5a, Trpv1, P2ry2* and *Chrm1* (Fig. S5A). ELAVL1 has predicted binding sites on almost all locally translated mRNAs regardless of axon specificity (Fig. S5A).

Fluorescence immunohistochemistry paired with particle analysis demonstrates that SFPQ protein is enriched in peripheral axons of the sciatic nerve (Fig. 7A,D), consistent with our prediction that SFPQ preferentially binds to mRNAs in the peripheral axons. In contrast, we find that SRSF10 protein is equally present in both central axons of the dorsal root and peripheral axons of the sciatic nerve (Fig. 7B,D). The third RBP tested, ELAVL1, is present in both the dorsal root and the sciatic nerve but is largely restricted to the nuclei of glia and other supporting cells (Fig. 7C,D). Thus, both SFPQ and SRSF10 are appropriately localized to contribute to trafficking and translation of mRNAs in axons, but only SFPQ is appropriately located to promote selective sorting towards the peripheral axon. Interestingly, our data also indicate another difference between the RBP puncta in the central versus peripheral axons: the puncta of SFPQ and SRSF10 were consistently larger within the sciatic nerve than in the dorsal root. This difference in size of the RBP-puncta suggest that there may be distinct features of RNP granules in each axon (Fig. 7E).

Select RBPs guide the axonal sorting and transport of functional RNA regulons

To determine whether SRSF10 and SFPQ bind and sort mRNAs for axonal translation, we performed RNA Immunoprecipitation paired with sequencing (RIP-Seq) in DRG neurons. In our experiments, SRSF10 and SFPQ protein were immunoprecipitated from DRG neurons grown in culture for 5 days, and mRNAs from these immunoprecipitates and from Rabbit IgG negative controls were extracted and sequenced (Table S12). We identified the mRNAs that are significantly enriched in the immunoprecipitates compared to the inputs. The mRNAs enriched in the SFPQ and SRSF10 immunoprecipitates include transcripts encoding several ion channels and receptors that we show are

locally translated within axons, including *Hcn1*, *Scn2a*, *Scn11a*, and *Catsper2* (Fig. 7F,G; Tables S13, S14).

We compared the RNAs enriched in the RBP immunoprecipitates with the translatome datasets. Among the mRNAs sequenced in the RBP-immunoprecipitates, we found that SFPQ binds 32 transcripts from the peripheral axon translatome, and 5 transcripts from the central axon translatome. Chi-square analysis indicated that SFPQ binds transcripts from peripheral axons at a rate significantly higher than expected when compared to the numbers in the peripheral axon and central axon translatomes (304 vs. 225) (Fig. 7H). The SFPQ-bound transcripts were enriched in biological processes relating to neuronal projection organization and assembly, including the distal axon, growth cone, and synapse (Fig. 7I, Table S15). Therefore, SFPQ may be implicated in selective mRNA sorting to the peripheral axon. In contrast to SFPQ, Chi-square analysis indicated that SRSF10 binds transcripts from each of the two axons with a distribution that is consistent with the numbers of mRNAs in the peripheral axon and central axon translatomes. These data indicate that SRSF10 may enable axonal mRNA transport, but it does not appear to be selective for one axon or the other. The top biological processes for the SRSF10-bound mRNAs are related to mRNA processing and splicing. However, these mRNAs were also enriched for transcripts encoding multiple components present in the axons, namely the presynaptic active zone, calcium channel complexes, and microtubule motor complexes (Fig. 7J,J'; Table S16). Taken together, these data implicate both SFPQ and SRSF10 in the axonal transport and organization of RNA regulons critical for axonal function. But only SFPQ may play an additional novel role in sorting mRNAs for selective trafficking and/or stabilization in the peripheral axons.

DISCUSSION

Spatial translatomics and high-resolution microscopy have revolutionized our ability to identify locally translated mRNAs and understand both the underlying mechanisms and the functional consequences of these subcellular specializations. Here we show that neuronal axon projections from the same cell can have distinct translatomes to fulfill specialized functional requirements. Our studies have begun to reveal the logic behind axonal sorting of select mRNAs; the RBP, SFPQ, preferentially binds the 3'UTRs of mRNAs that are translated in the peripheral axons and is enriched in RNPs localized within the peripheral axons of the sciatic nerve. The set of mRNAs that are locally translated in the peripheral and central axons include multiple ion channels and receptors related to neuronal firing, nociceptive processing, and regenerative capacity of sensory neurons. Thus, regulated translation has the potential of selectively and dynamically modifying signal transmission within individual axon branches.

Perhaps surprisingly, our studies indicate that many mRNAs that are translated within axons encode plasma membrane-bound ion channels and receptors. It is therefore appropriate to question whether axons are capable of the translational and secretory pathways required for membrane targeting and integration. Early electron microscopy studies did not detect ribosomes, rough endoplasmic reticulum, or Golgi apparatus in axons [50]. More recently, monosomes, small diameter ER tubules, and Golgi satellites have been identified in peripheral axons [16,44,51–54]. It has been suggested that axonal ion channels can be shuttled from axonal Golgi satellites to the plasma membrane through Rab6-positive exocytic vesicles [55]. In addition, atypical, membrane proteins that are core-glycosylated rather than N-glycosylated may bypass the Golgi apparatus and be more directly shuttled to the axonal plasma membrane [56,57]. Indeed, both the peripheral and central axonal translatomes include glycosylating enzymes (*Galnt5* in peripheral axon dataset and *St6galnac2* in central axon dataset). Several key locally translated mRNAs identified here, including *Scn2a, Gabrb3*, and *Grin2a,* encode proteins that have been observed to be core-glycosylated in axonal membranes [56]. Taken together, specialized axonal translation, processing, and secretion of membrane bound ion channels and receptors is both feasible and likely in distant axons.

It has been shown that differential ion channel insertion in axonal membranes controls neuroplasticity by altering membrane composition [58–60], however, there is little previous evidence that mRNA transport and regulated axonal translation contribute to dynamic changes of axonal physiology. Genes encoding voltage-gated sodium channels are among the membrane embedded proteins that are locally translated in the axons. There are nine distinct genes that encode different voltage-gated sodium channels, Nav1.1–1.9 [61], and individual neurons of the CNS and PNS each express a subset of these channel genes [40,62,63].

While somatosensory neurons are known to express distinctive sodium channels, previous modeling studies of somatosensory electrophysiology have assumed that the channel composition within the central and peripheral axons are similar [64,65]. Our data indicate that *Scn2a*, which encodes Nav1.2, is translated in peripheral axons, while *Scn11a*, which encodes Nav1.9, is translated in the central axons. Nav1.2 is a tetrodotoxin-sensitive (TTX) channel with fast kinetics, while Nav1.9 is a slowly activating/ inactivating, TTX-resistant channel that amplifies subthreshold signals [40,62,63,66,67]. In addition to the selective local translation of individual sodium channels, we find that the Hyperpolarization Activated Cyclic Nucleotide Gated Potassium Channel 1 (HCN1) is also selectively translated in the peripheral axons. HCN1 exhibits rapid kinetics, enhances action potential initiation and enables increased action potential frequency [68–70]. Peripheral axons resemble dendrites in that they are the site of initial stimulation and signal integration[71] and so we hypothesize that HCN1 and Nav1.2 may facilitate similar functions in CNS dendrites and DRG peripheral axons to enable initiation and propagation of action potentials. Conversely, Nav1.9 is predominantly expressed in nociceptive neurons in the PNS, where it may amplify subthreshold pain signals in the central axon and so adjust the electrophysiologic input to the spinal cord[40]. In fact, loss or mutations of Nav1.9 in sensory neurons disrupt inflammatory and cold-triggered pain sensation in mice and humans [40,72,73], while gain-of-function mutations in humans resulted in episodic cold pain sensation and painful peripheral neuropathy [40]. Similarly, *Hcn1* null mice, with loss of HCN1 in sensory neurons, showed reduced neuropathic pain with less cold allodynia than wild-type mice after nerve injury [74]. Therefore, precise control over *Scn11a* and *Hcn1* localization and translation is likely required for appropriate pain sensation and may play a prominent role in neuropathic pain syndromes [72,73].

Components of a voltage-dependent, pH sensitive calcium channel that is highly expressed in sperm, *Catsper2, Catsperd and Catsperζ*[32], were identified in the TRAP-Seq dataset of the peripheral axon. RNAscope validated that Catsper2 mRNA is enriched in the peripheral axons, while data from RIP-Seq indicate tha*t Catsper2* is one of the transcripts bound by SRSF10, an RBP present in both central and peripheral axons. Previous single cell sequencing studies from both mouse and human DRGs have demonstrated that Catsper2 is expressed in the Calca+ nociceptive neurons [23,75,76]. Due to the lack of a validated antibody, we could not use PLA to verify local translation of Catsper2 in the peripheral axons. Nonetheless, these findings suggest that translation of specialized calcium channels may also contribute to differential physiology of the central and peripheral axons of somatosensory neurons.

In addition to localized translation of voltage-gated sodium, calcium, and HCN channels, we demonstrate that mRNA encoding the serotonin receptor, 5-HTR3A, is selectively located and translated in central axons, indicating that serotonergic signals in the spinal cord directly modulate primary somatosensory inputs. Indeed, axons from serotonergic neurons of the raphe nuclei are known to descend to the dorsal horn of the spinal cord, and ~15% of axo-axonic contacts with DRGs are serotonergic [77,78]. Previous models have suggested that descending serotonergic inputs directly modulate GABAergic interneurons in the dorsal horn, which express excitatory 5-HTR3A receptors [37,38]. Therefore, adjustments of pain signaling and sensation within the excitatory, glutamatergic central axon terminals may provide an important initial site of pain facilitation instead of inhibition. Together, localized translation of 5-HTR3A and other ion channels may enable the peripheral axons to integrate and accurately propagate action potentials initiated in the periphery and the central axons tune and refine the signals conveyed to the CNS [78,79].

Another major distinction between central and peripheral axons of DRG neurons is the capacity for peripheral axons to regenerate after injury, while central axons cannot do so. Peripheral nerve regeneration depends on both neuron-intrinsic components and signaling pathways initiated by glial and immune cells in the local microenvironment [80,81]. Our translatomic analyses reveal that peripheral axons locally translate multiple ciliary basal body and ribosomal proteins, which are not seen in the central axon translatome. Signaling within the primary cilium can modulate axon growth cone and tract formation[33] and ciliary proteins organize microtubule assembly and protein transport. For example, the ciliary protein, Pifo, promotes cytoskeletal protein and kinesin motor protein binding [82], Lca5 is implicated in protein transport [83], and Odf2l and Sdccag8 are found in the microtubule organizing center [84,85]. Cytoskeletal changes including microtubule polymerization and formation of a growth cone are essential features in axon regeneration [81]. Thus, the local regulation of Pifo, Lca5, Odf2l and Sdccag8 may contribute to the ability

of peripheral axons to efficiently reorganize the cytoskeleton and enable a regenerative response. Furthermore, local synthesis of ribosomal components in peripheral axons may facilitate ribosomal repair, a function that has been linked to dynamic responses to mechanical injuries or other cell stresses[35]. Together localized regulation and synthesis of cytoskeletal outgrowth and translational machinery provide peripheral axons with adaptive flexibility that may aid in regenerative processes in response to nerve injury.

A key question addressed here is how specific RNA regulons, or subsets of functionally related mRNAs with synchronized expression, are coordinately transported and sorted to a specific axon. RBPs are known to regulate RNA regulons at the level of splicing, export, transport, localization, and stability [86]. It has been shown that co-regulation of RNA regulons by specific RBPs is required for axon viability [25,87]. In this study, we implicated several RBPs in the organization of central and peripheral axonal translatomes. SFPQ and SRSF10 were initially identified as RNA splicing factors containing both RNA recognition motifs (RRMs) and intrinsically disordered regions [88–90]. In addition to its role in splicing, SFPQ has been identified as a component of axonal RNP granules and enables axonal transport of mRNA cargoes [25,91–93]. While less is known about SRSF10, it has been shown to regulate metabolic processes such as glycolysis [94], and has also been functionally linked to neurogenesis and spermatogenesis [95–97]. Here we show that SFPQ and SRSF10 bind multiple locally translated mRNAs and that the subcellular distribution of these two components are strikingly different, with SFPQ enriched in peripheral axons and SRSF10 present in both central and peripheral axons. RIP-Seq analysis revealed several potential RNA regulons that may be coordinated by SFPQ and SRSF10[2,25], including mRNAs needed for neuron projection organization, motor protein coordination, and presynaptic active zone complexes. Future studies will be needed to determine whether SFPQ and SRSF10 granules rely on direct interaction with kinesin motors [98–100], and/or hitchhike on membrane enclosed organelles for differential targeting of RNA regulons to the peripheral and central axons [101,102].

To our knowledge, SFPQ is the first identified RBP involved in selective axonal mRNA sorting. This novel role joins a host of cytoplasmic functions qualifying SFPQ as a master regulator of axonal survival[91]. For example, in peripheral neurons, SFPQ directly binds a kinesin complex containing the motor, KIF5A, and adaptor, KCL1, to transport mRNAs encoding axonal survival factors, such as *Laminb2* and *Bclw,* along microtubules [25,98,100]. Indeed, both SFPQ knockdown and selective interruption in transport activity led to axon degeneration in sensory neurons, implying SFPQ transport of mRNAs encoding survival factors is necessary for their local translation and function. However, it is not known whether SFPQ granules orchestrate peripheral sorting of survival factors at the level of 3'UTR motif recognition, kinesin binding availability, and/or preference for differential microtubule organizations. For instance, while central and peripheral axons both display plus-ends out microtubule polarity, the central axon has increased Δ2 tubulin levels affecting mitochondrial motility and trafficking of multiple cargoes [21]. In fact, cytoplasmic aggregation of SFPQ is implicated in several neurodegenerative disorders including, frontotemporal lobar degeneration (FTLD), and Alzheimer's disease, as well as sensory neuropathies including chemotherapy-induced peripheral neuropathy, and SFPQ mutations can cause amyotrophic lateral sclerosis (ALS) [91–93]. Given the importance of SFPQ in the localization of axonal RNA regulons, disruption of SFPQ RNA granule transport and sorting is likely to play an important role in the pathogenesis of multiple axonal degenerative diseases.

The comprehensive comparisons of central and peripheral axon translatomes in DRG neurons assembled here provide critical resources for understanding the basis of compartmentalized neural function. These axonal translatomes reveal that functional characteristics such as electrophysiologic properties, can be rapidly and locally modulated by changes in translation in response to environmental cues. Identification of distinct RBPs that coordinate and guide intracellular transport and translation of RNA regulons reveal key components that determine the asymmetry of neuronal projections required for functional circuitry across distinct biological spheres.

Limitations of the study

Due to constraints in the TRAP protocol, we were limited to pooling both male and female mice at postnatal week 1 to generate sufficient material for TRAP sequencing. While pooling across sexes increased the sample size, it also introduced the potential for masking or confounding sex-based

biological differences in gene expression. Future studies that separate male and female mice or incorporate sex as a biological variable could provide more detailed insights into sex-specific differences in axons. Additionally, by focusing exclusively on young mice, our dataset represents a snapshot of early postnatal development, limiting our ability to assess how disease processes affect the local translatome later in life [103]. The central axon dissection, which included both dorsal roots and spinal cord, also contained DRG axon terminals, while the peripheral dissection focused on the sciatic nerve from the ganglia to the knee, excluding axon terminals in the skin and footpads. This limitation may have hindered the detection of mRNAs encoding receptors such as Trpv1, Ntrk1, and Asic3 in peripheral axons. Moreover, all in vivo work was conducted within Nav1.8+ DRG neuron populations. The strict confidence interval of our bioinformatic approach filtered out mRNAs that may be locally translated, particularly those that may be translated both in Nav1.8+ axons and in surrounding cells. While Nav1.8+ neurons encompass almost all nociceptive subtypes, they also include C-fiber low-threshold mechanoreceptors (C-LTMRs), non-nociceptive high-threshold mechanoreceptors (C-HTMRs), pruriceptors, thermoreceptors, and others [19,23]. As a result, our dataset does not specifically focus on nociceptors.

RESOURCE AVAILABILITY

Lead Contact

- Requests for further information and resources should be directed to the lead contact, Rosalind Segal (Rosalind_segal@dfci.harvard.edu).

Materials Availability

- This study did not generate new unique reagents.

Data and code availability

- TRAP-seq and RIP-seq data have been deposited at GEO:GSE289550 and GEO:GSE289551 and will be publicly available as of the date of publication.
- TRAP-seq data are also available for browsing and analysis via the Pain-seq multi-omic data resource at http://painseq.shinyapps.io/CompartmentTRAP/.
- Novel code used to generate the web resource has been deposited to GitHub (http://github.com/Renthal-Lab/CompartmentTRAPShiny).
- Any additional information required to reanalyze the data reported in this paper is available from the lead contact upon request.

ACKNOWLEDGEMENTS

RNA Sequencing was performed in the University of California-San Francisco Genomics CoLab by Michael Adkisson, Andrew Schroeder, Andrea Barczak, and Walter Eckalbar. RIP Sequencing was performed by the MBCF: Genomics Core Facility at Dana-Farber Cancer Institute by Zack Herbert and Maura Berkeley. This work was supported by NIH grants R01-NS050674 and R01-CA205255 (RAS) and T32-AG000222 (ES). We thank David Ginty, Mike Greenberg, and Charles D Stiles for helpful comments on the manuscript, and Myriam Heiman, Sarah Pease-Raissi, and Ozge Tasdemir-Yilmaz for help with TRAP-Seq methods.

AUTHOR CONTRIBUTIONS

ESS conceptualized and designed the study, performed the experiments, analyzed the data, and wrote the manuscript. EN assisted with tissue processing, performed immunohistochemical experiments, ran bioinformatic analysis, and reviewed and edited the manuscript. MFP provided technical expertise, maintained mouse colonies, and reviewed and edited the manuscript. JZP assisted with tissue processing, conducted immunohistochemical experiments, and review and edited the manuscript. SAB developed the web resource. RAS conceptualized and designed the study, supervised the research, contributed to the data interpretation, and provided critical revisions to the manuscript.

DECLARATION OF INTERESTS

The authors declare no competing interests.

FIGURE TITLES AND LEGENDS

Figure 1. Overview of the local translatomes of somatosensory DRG neurons. A) Principal component analysis of DRG soma, peripheral axon, and central axon samples (n=4 peripheral and central axon samples, n=8 DRG soma samples). B) Venn diagram detailing the total number of mRNA transcripts in DRG soma, peripheral axon, and central axon translatomic datasets, as well as shared values. C-E). Volcano plots demonstrating the number mRNA transcripts with significantly higher expression in GFP+ TRAP samples from the peripheral axon (C), central axon (D), and DRG soma (E) as compared to GFP-negative control samples from the same tissue compartment (p.adj ≤ 0.05; fold-change ≥ 1). F) Venn diagram detailing the number of mRNA transcripts in DRG soma, peripheral axon, and central axon translatomic datasets after background filtering (i.e. removing transcripts with expression in GFP-negative control samples).

Figure 2. Functional annotation of the DRG soma translatome. A) Heatmap highlighting a cluster of genes with higher expression in GFP+ DRG soma translatome samples as compared to GFP-negative controls (n=8 samples/group). B) Gene ontology (GO) enrichment analysis visualized as a dot plot, where each dot represents a significantly enriched biological process (BP) from the DRG soma translatome dataset (p.adj ≥ 0.05). C) Heatmap highlighting a cluster of genes with higher expression in GFP-negative control samples as compared to GFP+ DRG soma translatome samples; this cluster largely contains non-specific mRNA transcripts from glial cells and non-nociceptive DRG subtypes which were ultimately filtered out of the DRG soma translatome gene set. D) Dot plot representing significantly enriched GO biological process within the GFP-negative control dataset (p.adj ≤ 0.05). Many of the background transcripts relate to non-neuronal processes, including extracellular matrix organization and gliogenesis.

Figure 3. Functional annotation of the peripheral axon translatome. A) Heatmap highlighting a cluster of genes with higher expression in GFP+ peripheral axon translatome samples as compared to GFP-negative controls (n=4 samples/group). B) Gene ontology (GO) enrichment analysis visualized as a dot plot, where each dot represents a significantly enriched cellular component (CC) from the peripheral axon translatome dataset (p.adj ≤ 0.05). There were no significant GO biological processes. C) A gene concept network demonstrates the color-coded linkages between genes from the peripheral axon translatome and significantly enriched GO terms. The size of the dot in the network correlates to the number of mRNAs in the peripheral axon translatome associated with that GO term. The local peripheral axon translatome encodes for genes related to synaptic specialization, cilia, and cytosolic ribosomal proteins.

Figure 4. Functional annotation of the central axon translatome. A) Heatmap highlighting a cluster of genes with higher expression in GFP+ central axon translatome samples as compared to GFP-negative controls (n=4 samples/group). B) Gene ontology (GO) enrichment analysis visualized as a dot plot, where each dot represents a significantly enriched biological process (BP) or molecular function (MF) from the central axon translatome dataset (p.adj ≤ 0.05). C) A gene concept network demonstrates the color-coded linkages between genes from the central axon translatome and significantly enriched GO terms. The size of the dot in the network correlates to the number of mRNAs in the central axon translatome associated with that GO category. The local DRG central axon translatome encodes for genes related to sensory perception, pain perception, and serotonin signaling.

Figure 5. Diverse membrane-associated ion channels are locally translated. A) Puromycin proximity ligation assay (Puro-PLA) enables *in situ* visualization of nascent protein in mouse tissues. Step 1: Puromycin injected into mice incorporates into the C-terminus of translating proteins, labeling nascent peptide chains. Step 2: PLA probes bind two targets of interest (i.e. Puromycin and ion channel) and enable amplification of a fluorescent signal if the targets are within 40 nm. B-E) Representative 20x fluorescent images of HCN1 (B), NAV1.2 (C), 5-HTR3A (D), and NAV1.9 (E) PLA puncta and TdTomato-labeled Nav1.8+ (Nav1.8-tdT) axons in dorsal roots and sciatic nerves, representing DRG central and peripheral axons, respectively. Scale bar = 40 µm. B'-E') Higher magnification images demonstrating the location and abundance of HCN1 (B'), NAV1.2 (C'), 5-HTR3A (D'), and NAV1.9 (E') puncta within Nav1.8-

tdT+ axons in the dorsal root and sciatic nerve. Scale bar = 10 µm. B''-E'') Quantification of the percent area occupied by HCN1 (B''), NAV1.2 (C''), 5-HTR3A (D''), and NAV1.9 (E'') PLA puncta within Nav1.8-tdT+ axons in dorsal roots and sciatic nerves. Statistical significance determined by two-way ANOVA with Tukey's multiple comparisons test and multiple unpaired t-tests (p-value ≤ 0.05). Data are represented as mean ± SEM. n=1-2 sciatic nerves samples/mouse and 1-3 dorsal roots samples/mouse from 4-5 mice.

Figure 6. Transcripts encoding locally translated ion channels have axon-specific expression. A-D) Representative 20x fluorescent images of *Hcn1* (A)*, Scn2a* (B), *Htr3a* (D), *and Scn11a* (D*)* mRNA puncta (visualized by RNAScope *in situ* hybridization) and TdTomato-labeled Nav1.8+ (Nav1.8-tdT) neurons in DRGs, dorsal roots and sciatic nerves, representing DRG soma, central axons, and peripheral axons, respectively. Scale bar = 100 µm (soma) and 40 µm (axons). A'-D') Higher magnification images demonstrating the location and abundance of *Hcn1* (A')*, Scn2a* (B'), *Htr3a* (D'), *and Scn11a* (D'*)* mRNA puncta within Nav1.8-tdT+ soma in the ganglia, and axon in the dorsal root and sciatic nerve. Scale bar = 10 µm. E-H) Quantification of the percent area occupied by *Hcn1* (E), *Scn2a* (F), *Htr3a* (G), and *Scn11a* (H) mRNA puncta within Nav1.8-tdT+ axons in dorsal roots and sciatic nerves. Statistical significance determined by two-way ANOVA with Tukey's multiple comparisons test and multiple unpaired t-tests (p-value ≤ 0.05). Data are represented as mean ± SEM. n=1-2 sciatic nerves samples/mouse and 1-3 dorsal roots samples/mouse from 4-5 mice.

Figure 7. Select RBPs orchestrate axon-specific mRNA transport. A-C) Representative 60x fluorescent immunohistochemistry images of SFPQ (A), SRSF10 (B), and ELAVL1 (C) protein in TdTomato-labeled Nav1.8+ (Nav1.8-tdT) axons in dorsal roots and sciatic nerves, representing DRG central and peripheral axons, respectively. The solid yellow box shows a 4x magnified image of the area surrounded by yellow dotted lines, demonstrating the location and abundance of protein within axons and nuclei of supporting cells. Scale bars: Full image = 40 µm; inlaid image = 10 µm. D, E) Quantification of the number (D) and size (E) of SFPQ, SRSF10, and ELAVL1-positive puncta within Nav1.8-tdT+ axons in dorsal roots and sciatic nerves. Statistical significance determined by two-way ANOVA with Tukey's multiple comparisons test. Data are represented as mean ± SEM. (n=1-2 sciatic nerves samples/mouse and 1-3 dorsal roots samples/mouse from 4-5 mice). F, G) Volcano plots from RIP-Seq experiments demonstrating the mRNA transcripts with significantly higher expression in SFPQ IP (F) and SRSF10 IP (G) samples as compared to the input fraction from the same DRG neuron cell culture experiments. Select locally translated mRNAs bound by SFPQ and SRSF10 are indicated on the volcano plots. (n= 4 sets; p.adj ≤ 0.05; fold-change ≥ 1). H) Contingency plot comparing the mRNAs found in SFPQ and SRSF10 RIP-Seq datasets. The bar graphs demonstrate the relative number mRNAs bound by SFPQ and SRSF10 (from RIP-Seq datasets) that were also locally translated in the central or peripheral DRG axons (from TRAP-Seq datasets). Statistical significance determined by Chi-square analysis: χ^2_c (d= 1; p ≤ 0.05) = 3.841; * = 6.097. I, J) Gene ontology (GO) enrichment analysis visualized as a dot plot, where each dot represents the most significantly enriched biological processes (BP), cellular compartments (CC), or molecular functions (MF) from the SFPQ IP (I) and SRSF10 IP (J) datasets (p.adj ≤ 0.05). J') Dot plot demonstrating significantly enriched, neuron-related GO cellular compartments from the SRSF10 IP dataset (p.adj ≤ 0.05).

SUPPLEMENTAL INFORMATION

Figure S1: Experimental details for spatial translatomics in DRG soma and axons. A) Nav1.8$^{Cre/+}$ mice were crossed to L10a-EGFP$^{fl/fl}$ mice to generate Nav1.8^{Cre};L10a-EGFP$^{fl/fl}$ mice and L10a-EGFP$^{fl/fl}$ negative control mice. In these mice, Nav1.8-Cre drives expression of an EGFP-tagged ribosomal subunit, L10a, selectively in a subset of DRG neurons. Tissue microdissections were performed in mice aged P1-3 to collect lumbar dorsal root ganglia (soma compartment), lumbar dorsal roots/ spinal cord (central axon compartment), and sciatic nerves (peripheral axon compartment). Using the Translating Ribosomal Affinity Purification (TRAP) protocol, ribosomal-associated mRNAs were isolated from tissue lysates using an anti-EGFP antibody immunoprecipitation followed by RNA extraction using filter columns. B) Endogenous L10a-EGFP expression is visible in the soma of DRG neurons and can be efficiently targeted and labeled by anti-GFP antibodies (scale bars: 40 µm (top row), 20 µm (bottom row). C). L10a-EGP protein can be immunoprecipitated from tissue lysates with anti-GFP antibodies. D) The purified

mRNA from 4 paired sets of TRAP and negative control samples were analyzed by ultra-low input RNA sequencing to elucidate the subcellular translatomes. A heatmap of pairwise comparisons demonstrates the similarities in the mRNA profiles from the same tissues and dissimilarity between samples from distinct tissues.

Figure S2. Locally translated ribosomal proteins in peripheral axons. A) There are four locally translated ribosomal proteins (encoded by Rps15a, Rpl7, Rps30/Fau, and Rps27a) in the peripheral axons of DRG nociceptors. The table depicts the proteins depth within the ribosome, location of ribosomal protein assembly, presence of a CUIC sequence motif, and whether local translation has previously been observed. B) Graphical depiction of 40s and 60s ribosome showing the depth and location of locally translated proteins in the peripheral axons. Figure adapted from Ben-Shem *et al.* (35).

Figure S3. Puromycin incorporation into DRG soma and axons. A) Representative fluorescent immunohistochemistry (IHC) images of Puromycin and TdTomato-labeled Nav1.8+ (Nav1.8-tdT) axons in DRG soma. Scale bar = 100 µm. B) Representative fluorescent images of Puromycin and Nav1.8-tdT+ axons in sciatic nerves. Yellow, orange, and green boxes denote areas with both Puromycin + TdTomato expression, only Puromycin expression, and only TdTomato expression, respectively. Scale bar = 40 µm. B') High magnification images of yellow, orange, and green boxes shown in (B). Scale bar = 10 µm.

Figure S4. Validation of mRNA expression of additional transcripts from translatomic datasets. A) qRT-PCR data demonstrating relative *Catsper2* mRNA expression in mouse testes (positive control), liver (negative control), DRG (soma), sciatic nerves (peripheral axons), and dorsal roots (central axons). All samples are normalized to GAPDH expression. Data are represented as mean ± SEM. B, C) Representative 20x fluorescent images of *Catsper2* (B) and *Trpv1* (C) mRNA puncta (visualized by RNAScope *in situ* hybridization) and TdTomato-labeled Nav1.8+ (Nav1.8-tdT) neurons in DRGs, dorsal roots, and sciatic nerves, representing DRG soma, central axons, and peripheral axons, respectively. Scale bar = 100 µm (soma) and 40 µm (axons). B', C') Higher magnification images demonstrating the location and abundance of *Catspser2* (B') and *Trpv1* (C') mRNA puncta within Nav1.8-tdT+ soma in the ganglia, and axons in the dorsal root and sciatic nerve. Scale bar = 20 µm (soma) and 10 µm (axons).

Figure S5. RNA Binding Protein motif analyses and localization. A) Heatmap displaying the number of RBP motifs within the 3'UTR of mRNAs with axon-preferential translation. RBPs identified via oRNAment, RNAmap, and RPS.renlab. B-D) STRING motif analysis of the cluster of RBPs found to have 3'UTR binding sites in: both central and peripherally targeted transcripts, i.e. "shared cluster" (B), centrally targeted transcripts, i.e. "central cluster" (C), and peripherally targeted transcripts, i.e. "peripheral cluster" (D). Data are represented as protein interaction networks with a high-confidence score of 0.700. Nodes represent individual proteins and are color-coordinated by enriched GO cellular components (FDR ≤ 0.05). Edges represent protein-protein associations based on known interactions, predicted interactions, and protein homology.

Figure S6. SFPQ and SRSF10 RIP-Sequencing. A, B) Western blot images showing SFPQ (A) and SRSF10 (B) protein . C) Principal component analysis demonstrating the variance between SFPQ IP, SRSF10 IP, IgG IP, and paired input samples (n=4 sets/condition). C') Principal component analysis demonstrating the variance between SFPQ IP (n=4 sets), SRSF10 IP (n=3 sets), and IgG IP (n=2 sets) samples with non-zero values only. D) Volcano plots from RIP-Seq experiments demonstrating the mRNA transcripts with significantly higher expression in IgG IP samples as compared to the input fraction from the same DRG neuron cell culture experiments. The most significant differentially expressed transcripts are labeled on the graph.

Supplemental Spreadsheets

Supplemental File1 (TRAP): Excel file containing Tables S1-S11, which are too large to fit in a PDF and related to TRAP-seq experiments.

Supplemental File2 (RIP): : Excel file containing Tables S12-16, which are too large to fit in a PDF and related to RIP-seq experiments.

STAR METHODS

EXPERIMENTAL MODEL AND STUDY PARTICIPANT DETAILS

Mouse Lines and Animal Care

All experimental procedures were conducted in accordance with the National Institutes of Health (NIH) guidelines and were approved by the Dana-Farber Cancer Institute (DFCI) Institutional Animal Care and Use Committee (IACUC).

Mouse Strains: L10a-eGFP$^{fl/fl}$ (B6;129S4-*Gt(ROSA)26Sor*$^{tm9(EGFP/Rpl10a)Amc}$/J) mice were the generous gift of Myriam Heiman (Massachusetts Institute of Technology) [24]. Nav1.8^{cre} (B6.129-Scn10a$^{tm2(cre)Jwo}$/H) and TdTomato$^{fl/fl}$ (B6.Cg-*Gt(ROSA)26Sor*$^{tm14(CAG-tdTomato)Hze}$/J) mice were kindly provided by David Ginty (Harvard Medical School). For *in vivo* TRAP studies, Nav1.8$^{cre/+}$ and L10a-eGFP$^{fl/fl}$ mice were crossed to generate Nav1.8^{cre};L10a-eGFP$^{fl/fl}$ mice (GFP+) and L10a-eGFP$^{fl/fl}$ (GFP-) littermate controls. For tissue collection and histology, Nav1.8^{cre} and TdTomato$^{fl/fl}$ mice were crossed to generate Nav1.8^{cre};TdTomato$^{fl/fl}$ mice with labelled sensory neurons.

Mice were group housed in a temperature-controlled environment (22 ± 2°C) with a 12-hour light/dark cycle and had free access to food and water. Mice aged P3-5 were used for all experiments. For TRAP experiments, 13-17 littermate animals of both sexes were pooled by genotype (GFP positive or negative) and used to generate TRAP samples. Pooling of both sexes was required to generate enough tissue material for TRAP-Sequencing. For tissue collection and histology, all TdTomato-expressing littermate animals of both sexes were used to generate tissue samples for downstream applications.

Primary Rat Cell Cultures

Timed pregnant Sprague-Dawley rats were purchased from Charles River for primary DRG neuron isolation. Embryos from timed pregnant Sprague-Dawley rats (aged E15) were used for primary cell culture isolation. All embryos, presumably of both sexes, were used. DRGs were dissected, dissociated, and plated in Matrigel (1:45; Thermo Fisher Scientific)-coated p35 dishes. DRG cultures were maintained in NeuroBasal medium supplemented with 2% B27, 1% Glutamax, 1% penicillin and streptomycin, 0.08% glucose, 1–100 ng/ml nerve growth factor (NGF)/brain-derived neurotrophic factor (BDNF; PeproTech), and 0.5 µM Cytarabine (AraC). Cultures were maintained in incubators at 37°C with 7.5% CO_2 for 5 days.

METHOD DETAILS

Translating Ribosomal Affinity Purification (TRAP)

TRAP protocol was adapted from Myriam Heiman [24]. Roughly 15 Nav1.8-Cre;L10a-eGFP mice aged P3-5 and L10a-eGP littermate controls were euthanized by CO_2 inhalation and cervical dislocation. Lumbar (L1-6) dorsal root ganglia (Soma), sciatic nerve (PA), and lumbar dorsal roots and spinal cords (CA) were quickly manually dissected in Dissection Buffer (1X HBSS, 2.5mM HEPES-KOH [pH7.4], 25mM Glucose, 4mM $NaHCO_3$, 100µg/mL cycloheximide) from pooled Soma and CA compartment tissues were immediately homogenized in ice-cold Polysome Extraction Buffer (20mH M HEPES-KOH [pH 7.4], 5mM $MgCl_2$, 150 mM KCl, 0.5mM DTT, 100µg/mL cycloheximide, protease inhibitors (EDTA-free), 40 U/mL RNAsin, 20 U/mL Superasin) using glass Dounce homogenizers. Pooled PA compartment tissue was enzymatically digested (0.1% Collagenase II, 0.2% Hyaluronidase, 40 U/mL RNAsin, 20 U/mL Superasin) in Dissection Buffer for 5 min at room temperature, then resuspended in ice-cold Polysome Extraction Buffer and Dounce homogenized. Homogenates were centrifuged for 10 minutes at 2,000 × *g*, 4 °C, to pellet large cell debris, and 1% NP-40 (AG Scientific, San Diego, CA) and 30 mM DHPC (Avanti Polar Lipids, Alabaster, AL) were added to the supernatant. After incubation on ice for 5 minutes, the lysate was centrifuged for 10 minutes at 20,000 × *g*, 4 °C. Supernatants were pre-cleared with unbound Pierce Protein L Magnetic Beads at 4 °C for 1 hour. Custom anti-GFP antibody (Htz-GFP-19C8; RRID:AB_2716737 and Htz-GFP-19F7; RRID:AB_2716736) coated Pierce Protein L Magnetic Beads were added to the supernatant and incubated at 4 °C with end-to-end rotation overnight. Beads were subsequently collected on a magnetic rack, washed three times with high-salt IP Wash Buffer (20 mM HEPES [pH 7.4], 350 mM KCl, 5 mM $MgCl_2$, 1% NP-40, 0.5mM dithiothreitol, 100 µg/ml cycloheximide, 3% bovine serum albumin [IgG Protease-free]) and immediately placed in Lysis Buffer with β-ME

(Absolutely RNA Nanoprep Kit) (Agilent Technologies, Santa Clara, CA) and incubated for 10 mins at room temperature. Eluted RNA in Lysis Buffer was removed from beads on a magnetic rack. RNA was further purified using the Absolutely RNA Nanoprep Kit with column purification and DNase digestion. RNA integrity and concentration was measured on an Agilent 2100 Bioanalyzer System with RNA 6000 Pico Kit (Agilent Technologies, Santa Clara, CA); amounts of RNA were estimated as <100pg for axon samples and <1ng for soma samples. Four biological replicates were performed for CA and PA tissues, and eight replicates were performed for somatic tissues.

Low Input Total RNA Sequencing and Analysis

Low input total RNA Sequencing (>10pg total RNA or 1-500 cells) was performed at the University of California-San Francisco Functional Genomics Core Facility. RNA libraries were prepared using the SMART-Seq v4 Mouse Kit (Takara Bio Inc.) and sequenced on an Illumina HiSeq 4000 instrument via 50bp sequencing. Sequences were aligned to mouse reference genome with STAR_2.7.2b [26]. RNA-seq analysis of raw counts was performed in R for sample-level quality control (principal component analysis), Differential Gene Expression testing for pairwise, group comparisons (DESeq2) [27], and Functional Annotation (GO) [28,29].

Puromycin Injection

Nav1.8^{cre};TdTomato$^{fl/fl}$ mice were injected with Puromycin Dihydrochloride (#P33020) (Research Products International, Mount Prospect, IL) at a concentration of 225mg/kg (0.9mg/mouse) delivered via intraperitoneal injection (30 µL in dH2O). After 25 min, mice were euthanized by CO_2 inhalation followed by cervical dislocation.

Mouse Histological Methods

Dorsal root ganglia (Soma), sciatic nerves (PA), and dorsal roots (CA) were rapidly dissected from euthanized mice in ice-cold 1X PBS and placed immediately fixed in 4% PFA overnight. Tissues were washed 3×5min with 1XPBS, then prepared for embedding with 10% to 30% sucrose gradient over 3 days, embedded in NEG-50 medium (VWR, Radnor, Pennsylvania), and sectioned at 16µm on a cryostat.

Proximity Ligation Assay

Proximity ligation was performed according to the Duolink In Situ Proximity Ligation (Millipore Sigma, Burlington, MA) protocol. In brief, 20µg of primary anti-Puromycin (Sigma, #MABE343; RRID:AB_2566826), anti-5HTR3A (Thermo Scientific, #MA512111; RRID:AB_10982728), anti-SCN11A (Alomone, #ASC-017; RRID:AB_2040200), anti-SCN2A (Alomone, #ASC-002; RRID:AB_2040005), and anti-HCN1(Alomone, #APC-056; RRID:AB_2039900) antibodies were conjugated to Duolink probes using the Duolink In Situ Probemaker Kit (Millipore Sigma, Burlington, MA). Frozen tissue sections were accommodated to room temperature for 30 mins. Slides were then permeabilized with 0.1% PBS-Triton-X-100 (PBST) and blocked with Duolink Blocking Solution. Conjugated primary antibodies were added to slides and incubated at 4 °C overnight. Duolink ligation and polymerization steps were performed to amplify fluorescent signal, followed by two wash steps. Coverslips were mounted with ProLong Gold Antifade Mountant complete with DAPI (ThermoFisher).

RNAscope In Situ Hybridization

In situ hybridization was performed according to the Co-detection Immunohistochemistry with RNAscope Fluorescent Multiplex Reagent (ACDBio, Burlington, MA) protocol for fixed-frozen tissue samples. In brief, sample slides were accommodated to room temperature for 30 mins. Sections were then prepared by washing with 1X PBS before baking for 30 mins at 60 °C. Sections were then post-fixed with 4% PFA for 15 minutes at 4 °C. Samples were dehydrated through serial incubations in 50%, 70%, and 100% Ethanol. Samples were treated with hydrogen peroxide for 10 min and then underwent antigen retrieval with RNAscope Target Retrieval Solution in a steamer basket for 5 minutes. Primary anti-RFP antibody (VWR, #RL600-401-379) was applied to slides and incubated at 4 °C overnight. Samples then underwent post-primary fixation in 4% PFA for 30 mins, followed by Protease Plus incubation for 30 mins in a HybEZ Oven at 40 °C, probe hybridization for 30 mins at 40 °C, AMP hybridization for 30 mins at 40 °C, HRP signal development for 15 mins at 40 °C, Opal 690 Reagent (Akoya Biosciences) incubation for 30 mins at 40 °C, and HRP blocking for 15 mins at 40 °C. Samples were then incubated with secondary antibody

(Invitrogen: AlexaFluor H+L) for 60 mins, followed by two wash steps. Coverslips were mounted with ProLong Gold Antifade Mountant complete with DAPI (ThermoFisher).

Fluorescent Immunohistochemistry

Fixed frozen sample slides were accommodated to room temperature for 30 mins. Samples were then permeabilized 3 x 5 min with 0.1% PBS-Triton-X-100 (PBST) and blocked with 5% donkey serum (in 0.1% PBST) for 1 hours at room temperature. Primary anti-RFP (VWR, #RL600-401-379), anti-SFPQ (Abcam, #ab38148), anti-SRSF10 (Bioss, #BS-13229R), and/or anti-HuR (Proteintech, #11910-1-AP) antibody were added to slides and incubated at 4 °C overnight. Slides were washed 3 x 3 min with 0.1% PBST and then incubated with secondary antibody (Invitrogen: AlexaFluor H+L) for 1 hour at room temperature, followed by additional wash steps. Coverslips were mounted with ProLong Gold Antifade Mountant complete with DAPI (ThermoFisher).

Confocal Microscopy and Image Analysis

All mouse histological methods were imaged on a Nikon Eclipse Ni C2 Si laser scanning upright confocal with 4 laser lines. Slides were imaged at 20x, 40x, and 60x magnification, acquired using NIS Elements software, and saved in nd2 format for further processing and analysis. Images were opened in ImageJ and subjected to basic preprocessing steps to enhance both Nav1.8+ axon and particle visibility; this included adjusting brightness and contrast and removing noise from the background by despeckling. A manual threshold was first applied to the Nav1.8+ axon channel, and a mask was generated from the selection and added as a region of interest (ROI). A manual threshold was then applied to the particle channel (displaying PLA, RNAscope, or IHC puncta), and the intensity values were adjusted to ensure clear delineation between the particles and the background. Once the appropriate threshold was set, the area of the image contained within the previously set ROI was converted into a binary mask. The Analyze Particles function was used to detect and quantify individual particles in the binary image. The analysis was performed with a size range of 1 - 100 pixels and circularity range of 0 -1.0. The results were output to a results table, which included measurements such as particle count, mean area, and standard deviation. Following automatic particle detection, the results were visually inspected to ensure accurate particle identification. If necessary, additional particles were manually added or removed from the analysis based on visual verification.

RNA Extraction and qRT-PCR

RNA was extracted from mouse testes, liver, dorsal root ganglia, sciatic nerves, and dorsal roots by basic phenol:chloroform extraction followed by isopropanol RNA precipitation. RNA was converted to cDNA with the High Capacity RNA-to-cDNA Kit (Applied Biosystems). Template cDNA and Catsper2 primers were incorporated into a SYBR Green master mixture (Applied Biosystems), and mRNA expression was quantified using the EP Gradient s Realplex Mastercycler (Eppendorf). GAPDH was used to normalize gene expression. Each sample was assessed in duplicate and included a template-free control. All primers used were synthesized by Eurofins.

RBP Bioinformatic Analysis

Bioinformatic RBP motif analysis of 3'UTRs were performed using the oRNAment and RBPmap databases [46,47]. The locally translated mRNAs associated with significant functional annotations were used as the input transcript reference list. Transcripts were limited to 3'UTRs. Predicted motif score cutoff was set to 90%. RBPs found to have binding motifs with the key 3'UTRs were further analyzed for their ability to form ribonucleoprotein granules using the RPS.renlab database [48]. Functional Annotation Analysis for RBP protein-protein interactions was performed using the STRING database [49]. The minimum required interaction score was set to High Confidence (0.700).

RNA Immunoprecipitation (RIP)

RNA Immunoprecipitation was performed according to the EZ- Magna RIP RNA-Binding Protein Immunoprecipitation (Millipore Sigma) protocol. In brief, on Day 5 of primary DRG neuron cell culture, cells were washed with ice-cold PBS and lysed at -80 °C overnight in Complete Lysis Buffer. Lysates were spun down to pellet cellular debris and the supernatant added to Protein A/G Beads conjugated with 5µg of primary anti-SFPQ (Abcam, #ab38148), anti-SRSF10 (MBL, #50304712), or anti-rabbit IgG (EZ-Magna Kit). Lysate-bead mixtures were incubated at 4 °C overnight with end-to-end rotation. Protein-RNA

complexes were eluted from beads in a Proteinase K Buffer for 30 mins at 55 °C. RNA was further purified using phenol:chloroform:isoamyl alcohol procedure followed by absolute ethanol and salt RNA precipitation.

RIP-Sequencing

Sequencing was performed by the DFCI MBCF:Genomics Core Facility using NovaSeq X: Low Input mRNAseq (>1ng RNA). Libraries were prepared with Takara SmartSeq v4 full length cDNA synthesis using oligo dT priming & 5' template switching enzyme. Sequencing was performed with 40M 150bp read pairs from Illumina NovaSeq X Plus. Sequences were aligned to rat reference genome with STAR_2.7.2b [26]. RNA-seq analysis of raw counts was performed in R for sample-level quality control (principal component analysis), Differential Gene Expression testing for pairwise, group comparisons (DESeq2) [27], and Functional Annotation (GO) [28,29].

Western blot

RBP immunoprecipitations for RIP experiments were confirmed by Western Blot. Post-IP (EZ-Magna kit protocol), lysates were separated by NuPAGE 4–12% Bis-Tris SDS-Page Protein Gels and probed with anti-SFPQ (1:1000; Abcam, #ab38148), and anti-SRSF10 (1:1,000; MBL, #50304712). Bands were visualized with Donkey anti-rabbit IgG (H+L)- HRP conjugated secondary antibodies (1:10,000; Bio-Rad; 1721019) and SuperSignal chemiluminescent substrates signal (Thermo Fisher Scientific). Blots were imaged using the AI600 Chemiluminescent Imager (GE Healthcare).

QUANTIFICATION AND STATISTICAL ANALYSIS

Statistical Methods

All statistical analyses were performed using RStudio and GraphPad Prism. Differential gene expression analysis was conducted using the RStudio DESeq2 package, which applies a Wald test with FDR adjusted p-values. All histological data were quantified in Prism and are represented as mean ± standard error of the mean (SEM). Grouped data with multiple comparisons were analyzed for statistical significance using two-way ANOVA with Tukey's multiple comparisons test. Contingency data were analyzed for statistical significance using Chi-Square. A P-value ≤ 0.05 was considered statistically significant. Data distribution was assumed to be normal, but this was not formally tested. Statistical details of experiments can be found in the figure legends.

ADDITIONAL RESOURCES

All raw and processed TRAP-seq and RIP-seq data from this study were deposited to Gene Expression Omnibus at GEO:GSE289550 and GEO:GSE289551 and will be made publicly available as of the date of publication.

The data are also available for browsing and analysis on the Pain-seq multi-omic data resource at http://painseq.shinyapps.io/CompartmentTRAP/, built using R Shiny (http://github.com/Renthal-Lab/CompartmentTRAPShiny).

REFERENCES

1. West, A. E., Griffith, E. C. & Greenberg, M. E. Regulation of transcription factors by neuronal activity. *Nature Reviews Neuroscience 2002 3:12* **3**, 921–931 (2002).
2. Keene, J. RNA regulons: coordination of post-transcriptional events. *Nat. Rev. Genet.* **8**, 533–543 (2007).
3. Cosker, K. E., Pazyra-Murphy, M. F., Fenstermacher, S. J. & Segal, R. A. Target-derived neurotrophins coordinate transcription and transport of bclw to prevent axonal degeneration. *J. Neurosci.* **33**, 5195–5207 (2013).
4. CE Holt, K. M. E. S. Local translation in neurons: visualization and function. *Nat. Struct. Mol. Biol.* **26**, 557–566 (2019).
5. Dalla Costa, I. *et al.* The functional organization of axonal mRNA transport and translation. *Nature Reviews Neuroscience 2020 22:2* **22**, 77–91 (2020).
6. Fernandopulle, M. S., Lippincott-Schwartz, J. & Ward, M. E. RNA transport and local translation in neurodevelopmental and neurodegenerative disease. *Nat Neurosci* **24**, 622–632 (2021).
7. Yoon, B. C. *et al.* Local translation of extranuclear lamin B promotes axon maintenance. *Cell* **148**, 752–764 (2012).
8. Cox, L. J., Hengst, U., Gurskaya, N. G., Lukyanov, K. A. & Jaffrey, S. R. Intra-axonal translation and retrograde trafficking of CREB promotes neuronal survival. *Nat. Cell Biol.* **10**, 149–159 (2008).
9. Sun, C. *et al.* The prevalence and specificity of local protein synthesis during neuronal synaptic plasticity. *Sci Adv* **7**, (2021).
10. Biever, A. *et al.* Monosomes actively translate synaptic mRNAs in neuronal processes. *Science (1979)* **367**, (2020).
11. Koenig, E. SYNTHETIC MECHANISMS IN THE AXON—IIRNA IN MYELIN-FREE AXONS OF THE CAT. *J Neurochem* **12**, 357–361 (1965).
12. Edström, A. THE RIBONUCLEIC ACID IN THE MAUTHNER NEURON OF THE GOLDFISH. *J Neurochem* **11**, 309–314 (1964).
13. Campbell, D. S. & Holt, C. E. Chemotropic responses of retinal growth cones mediated by rapid local protein synthesis and degradation. *Neuron* **32**, 1013–1026 (2001).
14. Garat, J., Di Paolo, A., Eastman, G., Castillo, P. E. & Sotelo-Silveira, J. The Trail of Axonal Protein Synthesis: Origins and Current Functional Landscapes. *Neuroscience* **567**, 195–208 (2025).
15. Jiménez-Díaz, L. *et al.* Local translation in primary afferent fibers regulates nociception. *PLoS One* **3**, (2008).
16. Merianda, T. & Twiss, J. Peripheral nerve axons contain machinery for co-translational secretion of axonally-generated proteins. *Neurosci Bull* **29**, 493–500 (2013).
17. Holt, C. E. Biological Roles of Local Protein Synthesis in Axons: A Journey of Discovery. *Annu Rev Genet* (2024) doi:10.1146/ANNUREV-GENET-072220-030822.
18. Jung, J. *et al.* mRNA transport, translation, and decay in adult mammalian central nervous system axons. *Neuron* **111**, 650-668.e4 (2023).
19. Meltzer, S., Santiago, C., Sharma, N. & Ginty, D. D. The cellular and molecular basis of somatosensory neuron development. *Neuron* **109**, 3736–3757 (2021).
20. Nascimento, A. I., Mar, F. M. & Sousa, M. M. The intriguing nature of dorsal root ganglion neurons: Linking structure with polarity and function. *Prog Neurobiol* **168**, 86–103 (2018).
21. Costa, A. C. *et al.* Axon-specific microtubule regulation drives asymmetric regeneration of sensory neuron axons. *Elife* **13**, (2025).
22. Schmidt, M. *et al.* Transcriptomic and proteomic profiling of NaV1.8-expressing mouse nociceptors. *Front Mol Neurosci* **15**, (2022).
23. Sharma, N. *et al.* The emergence of transcriptional identity in somatosensory neurons. *Nature* **577**, 392–398 (2020).
24. Heiman, M. *et al.* A translational profiling approach for the molecular characterization of CNS cell types. *Cell* **135**, 738–748 (2008).
25. KE Cosker, S. F. M. P.-M. H. E. R. S. The RNA-binding protein SFPQ orchestrates an RNA regulon to promote axon viability. *Nat. Neurosci.* **19**, 690–696 (2016).
26. Dobin, A. *et al.* STAR: Ultrafast universal RNA-seq aligner. *Bioinformatics* **29**, 15–21 (2013).
27. Love, M. I., Huber, W. & Anders, S. Moderated estimation of fold change and dispersion for RNA-seq data with DESeq2. *Genome Biol* **15**, (2014).

28. Aleksander, S. A. *et al.* The Gene Ontology knowledgebase in 2023. *Genetics* **224**, (2023).
29. Xu, S. *et al.* Using clusterProfiler to characterize multiomics data. *Nature Protocols 2024 19:11* **19**, 3292–3320 (2024).
30. Lu, W. *et al.* METTL14-mediated m6A epitranscriptomic modification contributes to chemotherapy-induced neuropathic pain by stabilizing GluN2A expression via IGF2BP2. *J Clin Invest* **134**, (2024).
31. Ramírez, D., Zúñiga, R., Concha, G. & Zúñiga, L. HCN Channels: New Therapeutic Targets for Pain Treatment. *Molecules: A Journal of Synthetic Chemistry and Natural Product Chemistry* **23**, 2094 (2018).
32. Quill, T. A. *et al.* Hyperactivated sperm motility driven by CatSper2 is required for fertilization. *Proc Natl Acad Sci U S A* **100**, 14869–14874 (2003).
33. Guo, J. *et al.* Primary Cilia Signaling Promotes Axonal Tract Development and Is Disrupted in Joubert Syndrome-Related Disorders Models. *Dev Cell* **51**, 759-774.e5 (2019).
34. Ben-Shem, A. *et al.* The structure of the eukaryotic ribosome at 3.0 Å resolution. *Science (1979)* **334**, 1524–1529 (2011).
35. Fusco, C. M. *et al.* Neuronal ribosomes exhibit dynamic and context-dependent exchange of ribosomal proteins. *Nat Commun* **12**, (2021).
36. Shigeoka, T. *et al.* On-Site Ribosome Remodeling by Locally Synthesized Ribosomal Proteins in Axons. *Cell Rep* **29**, 3605-3619.e10 (2019).
37. Das Gupta, R. R., Scheurer, L., Pelczar, P., Wildner, H. & Zeilhofer, H. U. Neuron-specific spinal cord translatomes reveal a neuropeptide code for mouse dorsal horn excitatory neurons. *Scientific Reports 2021 11:1* **11**, 1–18 (2021).
38. Heijmans, L., Mons, M. R. & Joosten, E. A. A systematic review on descending serotonergic projections and modulation of spinal nociception in chronic neuropathic pain and after spinal cord stimulation. *Mol Pain* **17**, 17448069211043964 (2021).
39. Parajulee, A. & Kim, K. Structural studies of serotonin receptor family. *BMB Rep* **56**, 527 (2023).
40. Dib-Hajj, S. D., Black, J. A. & Waxman, S. G. NaV1.9: a sodium channel linked to human pain. *Nat Rev Neurosci* **16**, 511–519 (2015).
41. Rosenbaum, T., Morales-Lázaro, S. L. & Islas, L. D. TRP channels: a journey towards a molecular understanding of pain. *Nature Reviews Neuroscience 2022 23:10* **23**, 596–610 (2022).
42. Wemmie, J. A., Taugher, R. J. & Kreple, C. J. Acid-sensing ion channels in pain and disease. *Nature Reviews Neuroscience 2013 14:7* **14**, 461–471 (2013).
43. Russo, A. F. & Hay, D. L. CGRP PHYSIOLOGY, PHARMACOLOGY, AND THERAPEUTIC TARGETS: MIGRAINE AND BEYOND. *Physiol Rev* **103**, 1565–1644 (2023).
44. Merianda, T. T. *et al.* A functional equivalent of endoplasmic reticulum and Golgi in axons for secretion of locally synthesized proteins. *Molecular and Cellular Neuroscience* **40**, 128–142 (2009).
45. S Das, R. S. Y. Y. The travels of mRNAs in neurons: do they know where they are going? *Curr. Opin. Neurobiol.* **57**, 110–116 (2019).
46. Benoit Bouvrette, L. P., Bovaird, S., Blanchette, M. & Lécuyer, E. ORNAment: A database of putative RNA binding protein target sites in the transcriptomes of model species. *Nucleic Acids Res* **48**, D166–D173 (2020).
47. Paz, I., Argoetti, A., Cohen, N., Even, N. & Mandel-Gutfreund, Y. RBPmap: A Tool for Mapping and Predicting the Binding Sites of RNA-Binding Proteins Considering the Motif Environment. *Methods Mol Biol* **2404**, 53–65 (2022).
48. He, Y. *et al.* RPS 2.0: an updated database of RNAs involved in liquid–liquid phase separation. *Nucleic Acids Res* **53**, D299–D309 (2025).
49. Szklarczyk, D. *et al.* The STRING database in 2023: protein-protein association networks and functional enrichment analyses for any sequenced genome of interest. *Nucleic Acids Res* **51**, D638–D646 (2023).
50. Chan-Palay, V. & Palay, S. L. Ultrastructural identification of substance P cells and their processes in rat sensory ganglia and their terminals in the spinal cord by immunocytochemistry. *Proc Natl Acad Sci U S A* **74**, 4050–4054 (1977).
51. Kersten, N. & Farías, G. G. A voyage from the ER: spatiotemporal insights into polarized protein secretion in neurons. *Front Cell Dev Biol* **11**, (2023).

52. Koppers, M. *et al.* Axonal endoplasmic reticulum tubules control local translation via P180/RRBP1-mediated ribosome interactions. *Dev Cell* **59**, 2053-2068.e9 (2024).
53. Kemal, S., Richardson, H. S., Dyne, E. D. & Fu, M. meng. ER and Golgi trafficking in axons, dendrites, and glial processes. *Curr Opin Cell Biol* **78**, 102119 (2022).
54. González, C. *et al.* Axons provide the secretory machinery for trafficking of voltage-gated sodium channels in peripheral nerve. *Proc Natl Acad Sci U S A* **113**, 1823–1828 (2016).
55. Cornejo, V. H. *et al.* Non-conventional Axonal Organelles Control TRPM8 Ion Channel Trafficking and Peripheral Cold Sensing. *Cell Rep* **30**, 4505-4517.e5 (2020).
56. Hanus, C. *et al.* Unconventional secretory processing diversifies neuronal ion channel properties. *Elife* **5**, (2016).
57. Bowen, A. B., Bourke, A. M., Hiester, B. G., Hanus, C. & Kennedy, M. J. Golgi-Independent secretory trafficking through recycling endosomes in neuronal dendrites and spines. *Elife* **6**, (2017).
58. Tyagi, S. *et al.* Compartment-specific regulation of NaV1.7 in sensory neurons after acute exposure to TNF-α. *Cell Rep* **43**, (2024).
59. Higerd-Rusli, G. P. *et al.* Inflammation differentially controls transport of depolarizing Nav versus hyperpolarizing Kv channels to drive rat nociceptor activity. *Proc Natl Acad Sci U S A* **120**, e2215417120 (2023).
60. Vacher, H. *et al.* Cdk-mediated phosphorylation of the Kvβ2 auxiliary subunit regulates Kv1 channel axonal targeting. *Journal of Cell Biology* **192**, 813–824 (2011).
61. Catterall, W. A., Perez-Reyes, E., Snutch, T. P. & Striessnig, J. International Union of Pharmacology. XLVIII. Nomenclature and structure-function relationships of voltage-gated calcium channels. *Pharmacol Rev* **57**, 411–425 (2005).
62. Bennett, D. L., Clark, X. A. J., Huang, J., Waxman, S. G. & Dib-Hajj, S. D. The Role of Voltage-Gated Sodium Channels in Pain Signaling. *Physiol Rev* **99**, 1079–1151 (2019).
63. Goodwin, G. & McMahon, S. B. The physiological function of different voltage-gated sodium channels in pain. *Nat Rev Neurosci* **22**, 263–274 (2021).
64. Graham, R. D., Bruns, T. M., Duan, B. & Lempka, S. F. Dorsal root ganglion stimulation for chronic pain modulates Aβ-fiber activity but not C-fiber activity: A computational modeling study. *Clin Neurophysiol* **130**, 941–951 (2019).
65. Sundt, D., Gamper, N. & Jaffe, D. B. Spike propagation through the dorsal root ganglia in an unmyelinated sensory neuron: a modeling study. *J Neurophysiol* **114**, 3140–3153 (2015).
66. Priest, B. T. *et al.* Contribution of the tetrodotoxin-resistant voltage-gated sodium channel Nav1.9 to sensory transmission and nociceptive behavior. *Proc Natl Acad Sci U S A* **102**, 9382–9387 (2005).
67. Herzog, R. I., Cummins, T. R. & Waxman, S. G. Persistent TTX-resistant Na+ current affects resting potential and response to depolarization in simulated spinal sensory neurons. *J Neurophysiol* **86**, 1351–1364 (2001).
68. Biel, M., Wahl-Schott, C., Michalakis, S. & Zong, X. Hyperpolarization-activated cation channels: from genes to function. *Physiol Rev* **89**, 847–885 (2009).
69. Kaupp, U. B. & Seifert, R. Molecular diversity of pacemaker ion channels. *Annu Rev Physiol* **63**, 235–257 (2001).
70. Roth, F. C. & Hu, H. An axon-specific expression of HCN channels catalyzes fast action potential signaling in GABAergic interneurons. *Nature Communications 2020 11:1* **11**, 1–10 (2020).
71. Goldstein, R. H. *et al.* Location and Plasticity of the Sodium Spike Initiation Zone in Nociceptive Terminals In Vivo. *Neuron* **102**, 801-812.e5 (2019).
72. Amaya, F. *et al.* The Voltage-Gated Sodium Channel Nav1.9 Is an Effector of Peripheral Inflammatory Pain Hypersensitivity. *The Journal of Neuroscience* **26**, 12852 (2006).
73. Lolignier, S. *et al.* The Nav1.9 Channel Is a Key Determinant of Cold Pain Sensation and Cold Allodynia. *Cell Rep* **11**, 1067–1078 (2015).
74. Momin, A., Cadiou, H., Mason, A. & Mcnaughton, P. A. Role of the hyperpolarization-activated current Ih in somatosensory neurons. *J Physiol* **586**, 5911–5929 (2008).
75. Bhuiyan, S. A. *et al.* Harmonized cross-species cell atlases of trigeminal and dorsal root ganglia. *Sci Adv* **10**, (2024).
76. Tavares-Ferreira, D. *et al.* Spatial transcriptomics of dorsal root ganglia identifies molecular signatures of human nociceptors. *Sci Transl Med* **14**, (2022).

77. Zhang, Y. *et al.* Identifying local and descending inputs for primary sensory neurons. *J Clin Invest* **125**, 3782–3794 (2015).
78. Hao, H. *et al.* Dorsal root ganglia control nociceptive input to the central nervous system. *PLoS Biol* **21**, e3001958 (2023).
79. Goldstein, R. H. *et al.* Location and Plasticity of the Sodium Spike Initiation Zone in Nociceptive Terminals In Vivo. *Neuron* **102**, 801-812.e5 (2019).
80. Feng, R., Saraswathy, V. M., Mokalled, M. H. & Cavalli, V. Self-renewing macrophages in dorsal root ganglia contribute to promote nerve regeneration. *Proc Natl Acad Sci U S A* **120**, e2215906120 (2023).
81. He, Z. & Jin, Y. Intrinsic Control of Axon Regeneration. *Neuron* **90**, 437–451 (2016).
82. Wang, L. & Dynlacht, B. D. The regulation of cilium assembly and disassembly in development and disease. *Development (Cambridge)* **145**, (2018).
83. Boldt, K. *et al.* Disruption of intraflagellar protein transport in photoreceptor cilia causes Leber congenital amaurosis in humans and mice. *Journal of Clinical Investigation* **121**, 2169–2180 (2011).
84. Donkor, F. F., Mönnich, M., Czirr, E., Hollemann, T. & Hoyer-Fender, S. Outer dense fibre protein 2 (ODF2) is a self-interacting centrosomal protein with affinity for microtubules. *J Cell Sci* **117**, 4643–4651 (2004).
85. Insolera, R., Shao, W., Airik, R., Hildebrandt, F. & Shi, S. H. SDCCAG8 Regulates Pericentriolar Material Recruitment and Neuronal Migration in the Developing Cortex. *Neuron* **83**, 805–822 (2014).
86. Keene, J. RNA regulons: coordination of post-transcriptional events. *Nat. Rev. Genet.* **8**, 533–543 (2007).
87. Lee, S. J. *et al.* hnRNPs Interacting with mRNA Localization Motifs Define Axonal RNA Regulons. *Mol Cell Proteomics* **17**, 2091 (2018).
88. Jumper, J. *et al.* Highly accurate protein structure prediction with AlphaFold. *Nature* **596**, 583–589 (2021).
89. Malaney, P., Benitez, O., Zhang, X. & Post, S. M. Assessing the role of intrinsic disorder in RNA-binding protein function: hnRNP K as a case study. *Methods* **208**, 59–65 (2022).
90. Choi, Y. *et al.* Time-resolved profiling of RNA binding proteins throughout the mRNA life cycle. *Mol Cell* **84**, 1764-1782.e10 (2024).
91. Lim, Y. W., James, D., Huang, J. & Lee, M. The Emerging Role of the RNA-Binding Protein SFPQ in Neuronal Function and Neurodegeneration. *Int J Mol Sci* **21**, 1–16 (2020).
92. Widagdo, J. *et al.* Familial ALS-associated SFPQ variants promote the formation of SFPQ cytoplasmic aggregates in primary neurons. *Open Biol* **12**, (2022).
93. Thomas-Jinu, S. *et al.* Non-nuclear Pool of Splicing Factor SFPQ Regulates Axonal Transcripts Required for Normal Motor Development. *Neuron* **94**, 322-336.e5 (2017).
94. Cai, J. *et al.* Targeting SRSF10 might inhibit M2 macrophage polarization and potentiate anti-PD-1 therapy in hepatocellular carcinoma. *Cancer Commun (Lond)* **44**, (2024).
95. Li, J. *et al.* SRSF10 regulates proliferation of neural progenitor cells and affects neurogenesis in developing mouse neocortex. *iScience* **26**, (2023).
96. Liu, W. *et al.* SRSF10 is essential for progenitor spermatogonia expansion by regulating alternative splicing. *Elife* **11**, (2022).
97. Ma, A. *et al.* SRSF10 regulates migration of neural progenitor cells and granule cells and affects the formation of dentate gyrus during the development of mouse hippocampus. *Neuroscience* **552**, 142–151 (2024).
98. Fukuda, Y. *et al.* Binding and transport of SFPQ-RNA granules by KIF5A/KLC1 motors promotes axon survival. *J Cell Biol* **220**, (2021).
99. Hirokawa, N. & Takemura, R. Molecular motors and mechanisms of directional transport in neurons. *Nat. Rev. Neurosci.* **6**, 201–214 (2005).
100. Guerra San Juan, I., Brunner, J. W., Eggan, K., Toonen, R. F. & Verhage, M. KIF5A regulates axonal repair and time-dependent axonal transport of SFPQ granules and mitochondria in human motor neurons. *Neurobiol Dis* **204**, 106759 (2025).
101. Strzyz, P. RNA granules take a ride on lysosomes. *Nat Rev Mol Cell Biol* **20**, 662 (2019).
102. Liao, Y. C. *et al.* RNA Granules Hitchhike on Lysosomes for Long-Distance Transport, Using Annexin A11 as a Molecular Tether. *Cell* **179**, 147-164.e20 (2019).

103. Megat, S. *et al.* Nociceptor Translational Profiling Reveals the Ragulator-Rag GTPase Complex as a Critical Generator of Neuropathic Pain. *Journal of Neuroscience* **39**, 393–411 (2019).

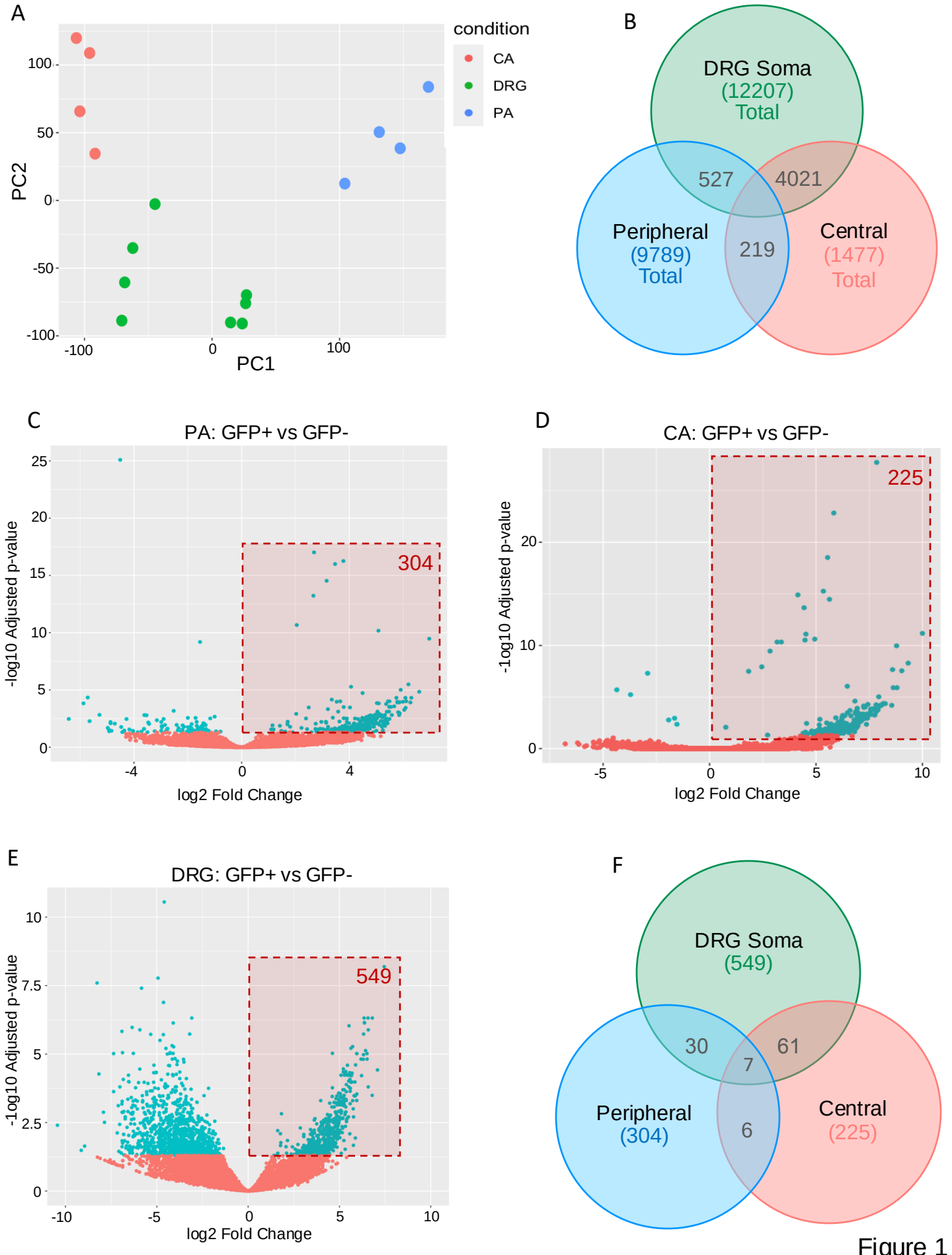
A
condition
CA
DRG
PA
PC2
PC1
100
50
0
-50
-100
-100
0
100
B
DRG Soma
(12207)
Total
527
4021
Peripheral
(9789)
Total
219
Central
(1477)
Total
C
PA: GFP+ vs GFP-
-log10 Adjusted p-value
log2 Fold Change
304
25
20
15
10
5
0
-4
0
4
D
CA: GFP+ vs GFP-
-1log10 Adjusted p-value
log2 Fold Change
225
20
10
0
-5
0
5
10
E
DRG: GFP+ vs GFP-
-1log10 Adjusted p-value
log2 Fold Change
549
10
7.5
5
2.5
0
-10
-5
0
5
10
F
DRG Soma
(549)
30
61
7
Peripheral
(304)
6
Central
(225)

Figure 1

TRAP-Seq Functional Annotation: DRG Soma (GFP+)

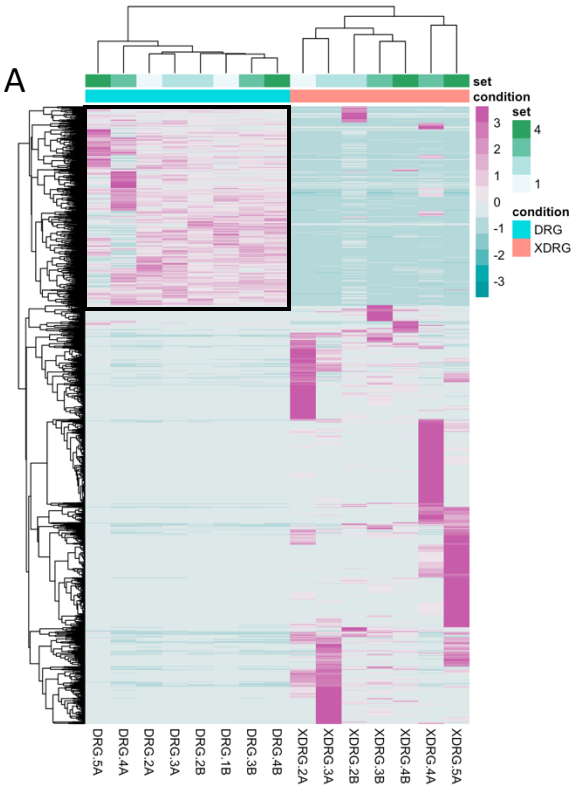

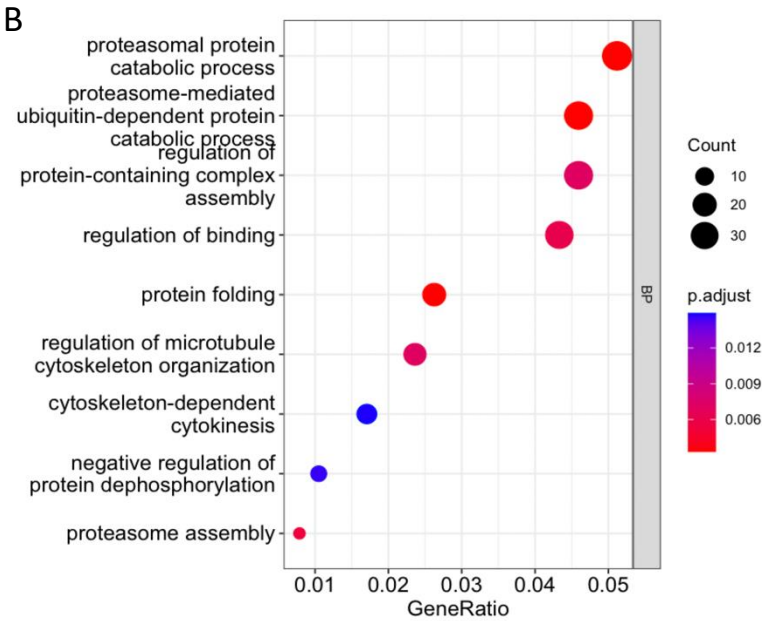

TRAP-Seq Functional Annotation: DRG Soma (GFP-)

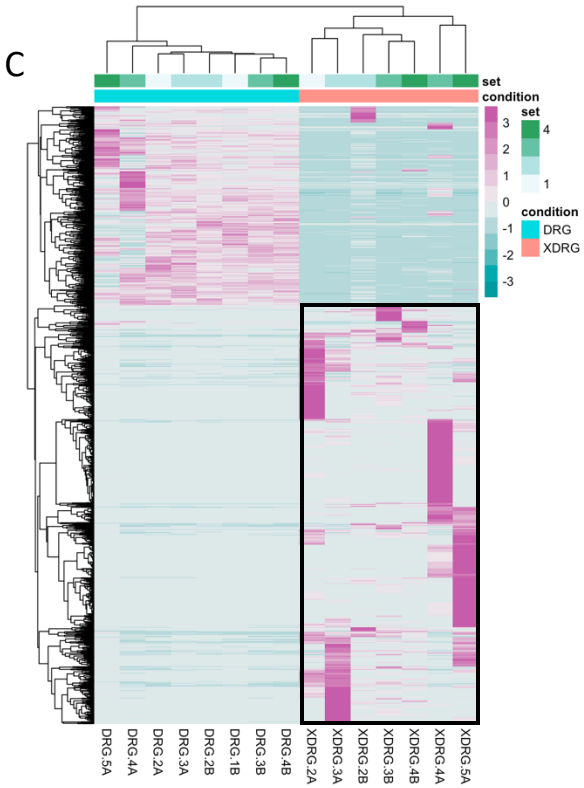

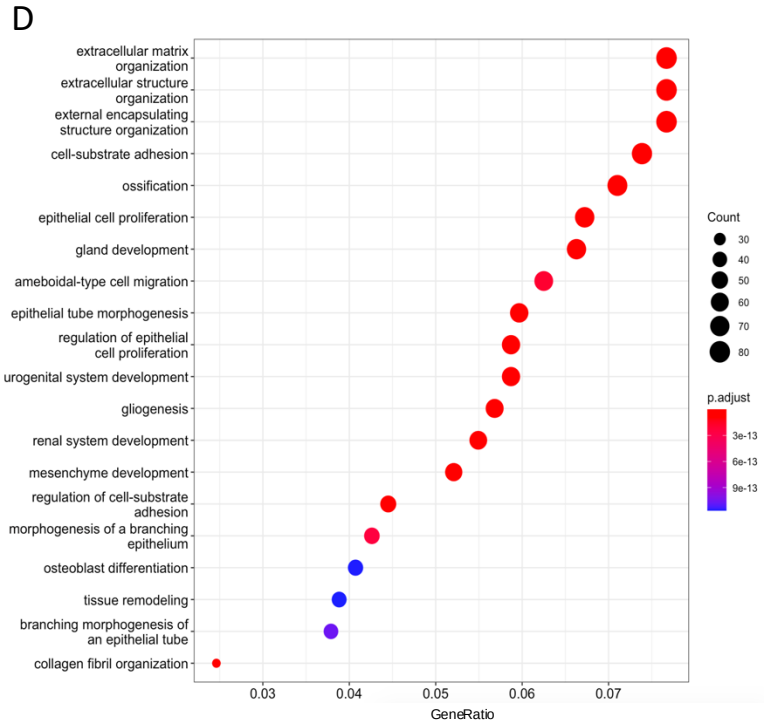

Figure 2

TRAP-Seq Functional Annotation: Peripheral Axon (GFP+)

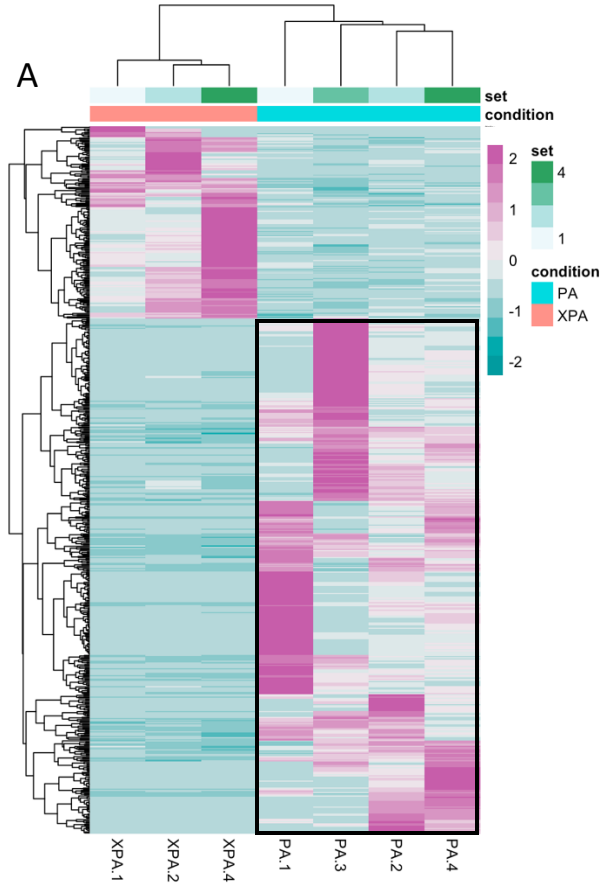

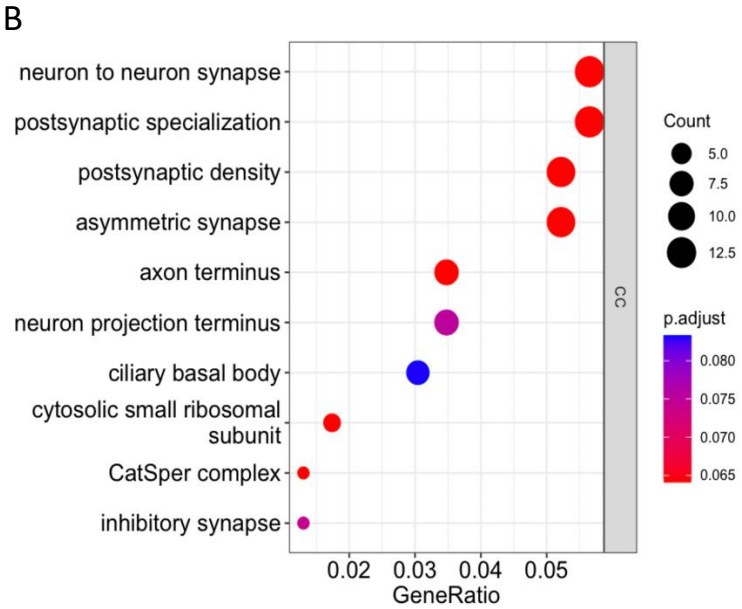

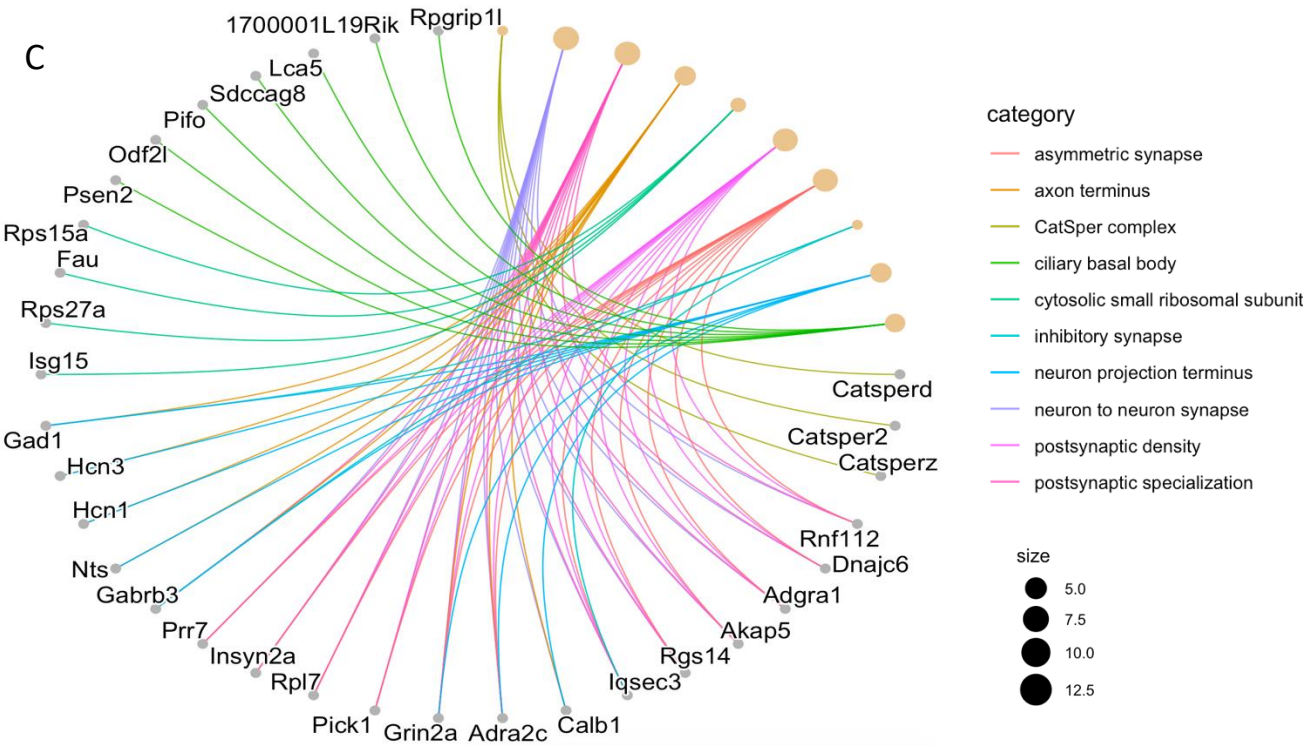

Figure 3

TRAP-Seq Functional Annotation: Central Axon (GFP+)

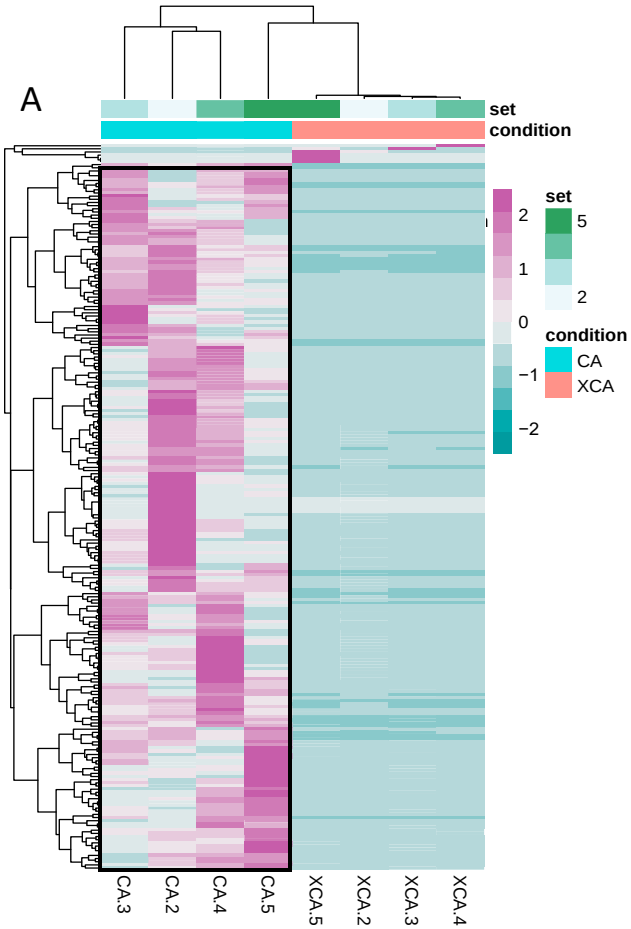

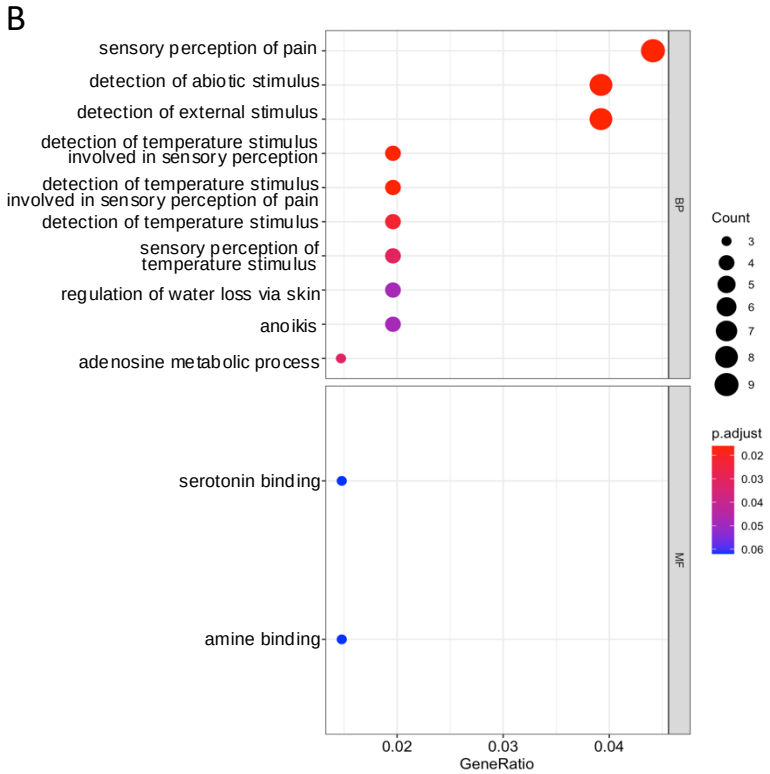

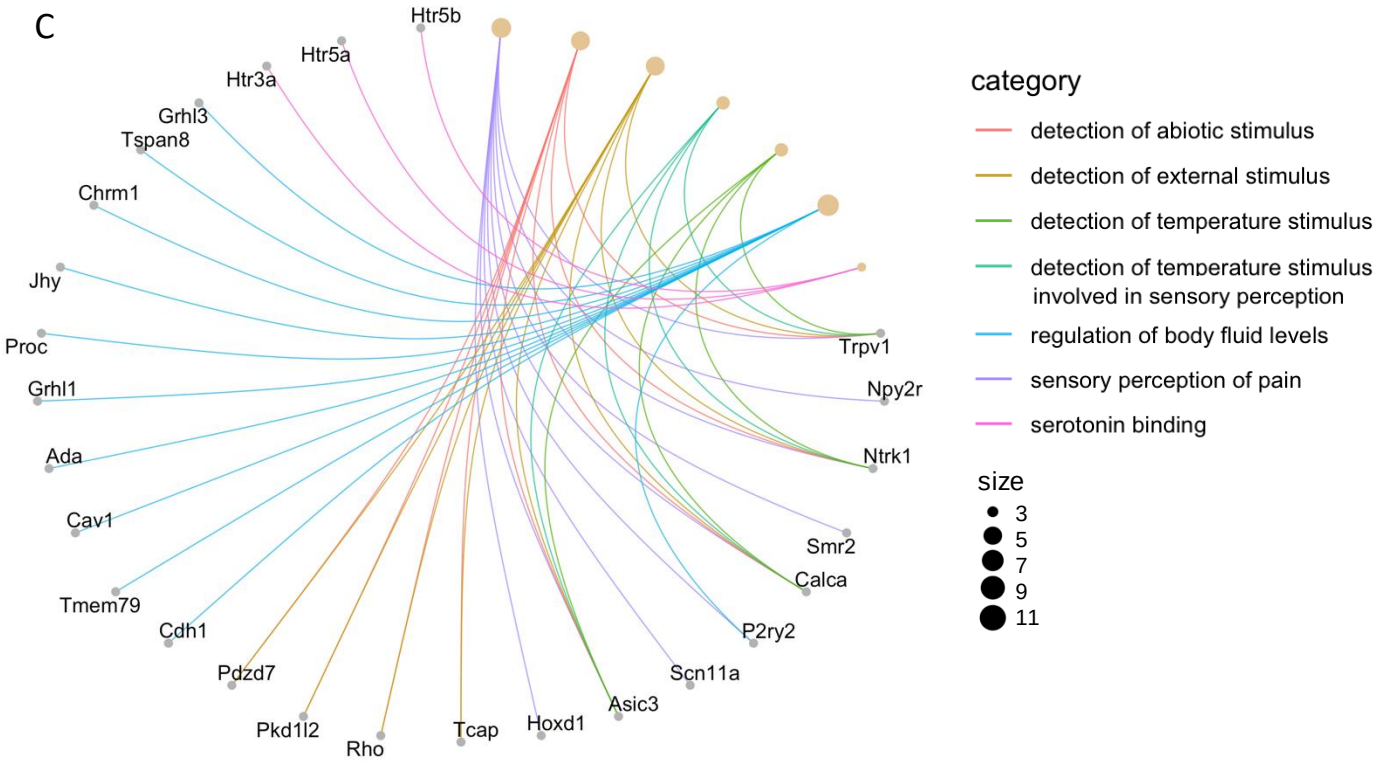

Figure 4

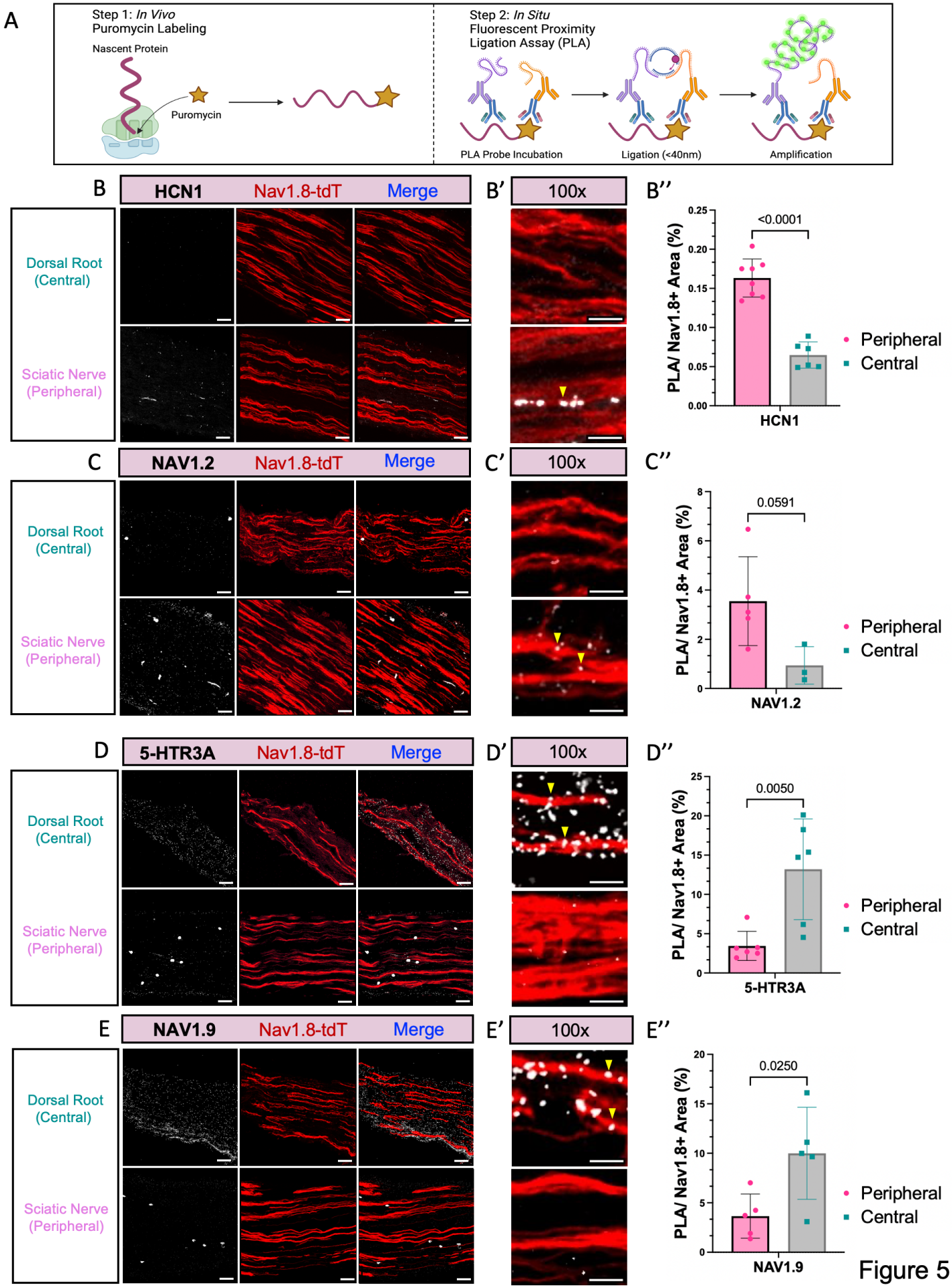
A
Step 1: In Vivo
Puromycin Labeling
Nascent Protein
Puromycin
Step 2: In Situ
Fluorescent Proximity
Ligation Assay (PLA)
PLA Probe Incubation
Ligation (<40nm)
Amplification
B
HCN1
Nav1.8-tdT
Merge
B'
100x
B''
Dorsal Root (Central)
Sciatic Nerve (Peripheral)
PLA/ Nav1.8+ Area (%)
<0.0001
HCN1
Peripheral
Central
C
NAV1.2
C'
C''
0.0591
NAV1.2
D
5-HTR3A
D'
D''
0.0050
5-HTR3A
E
NAV1.9
E'
E''
0.0250
NAV1.9

Figure 5

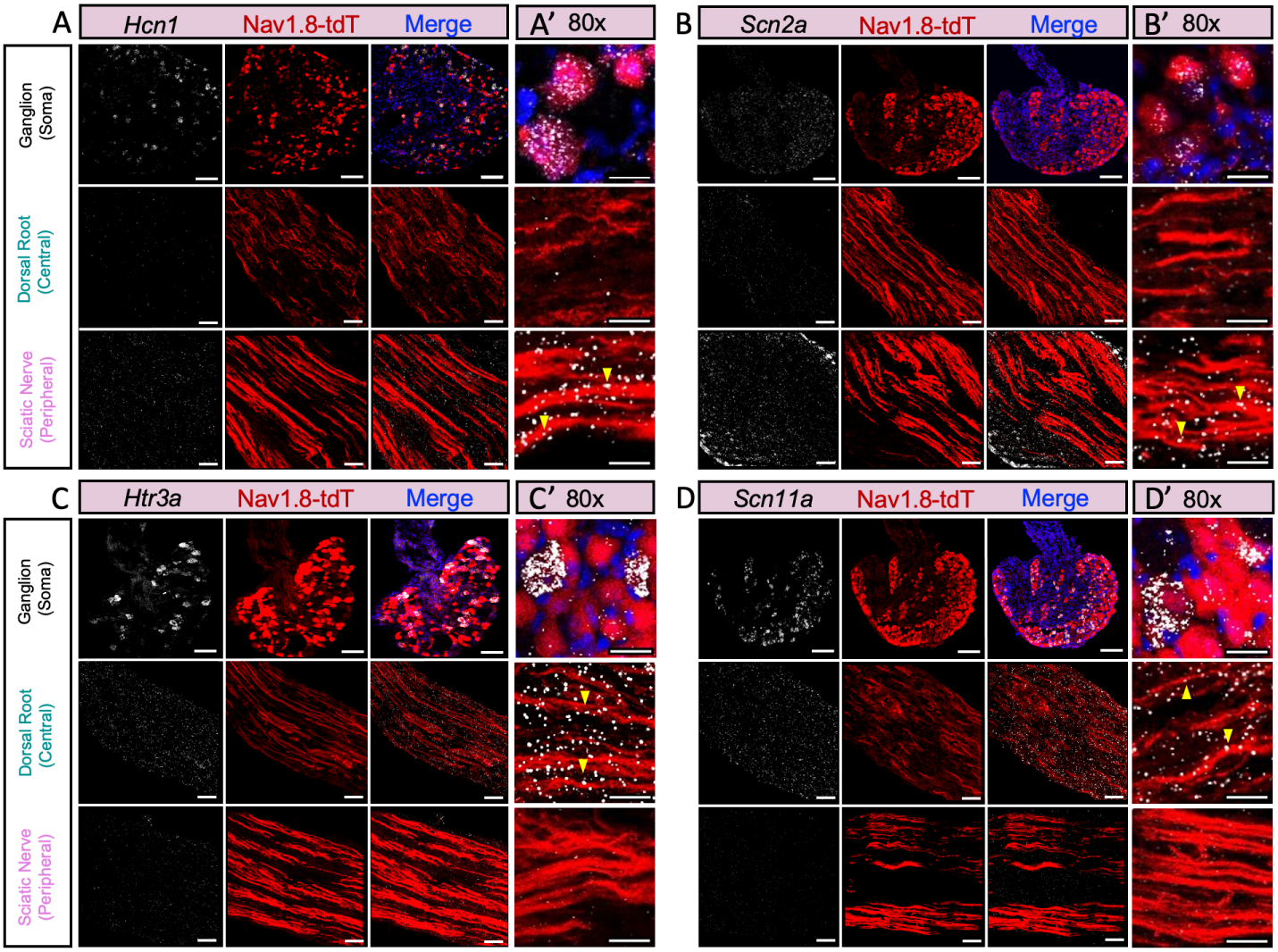
A
Hcn1
Nav1.8-tdT
Merge
A' 80x
B
Scn2a
Nav1.8-tdT
Merge
B' 80x
C
Htr3a
Nav1.8-tdT
Merge
C' 80x
D
Scn11a
Nav1.8-tdT
Merge
D' 80x
Ganglion (Soma)
Dorsal Root (Central)
Sciatic Nerve (Peripheral)

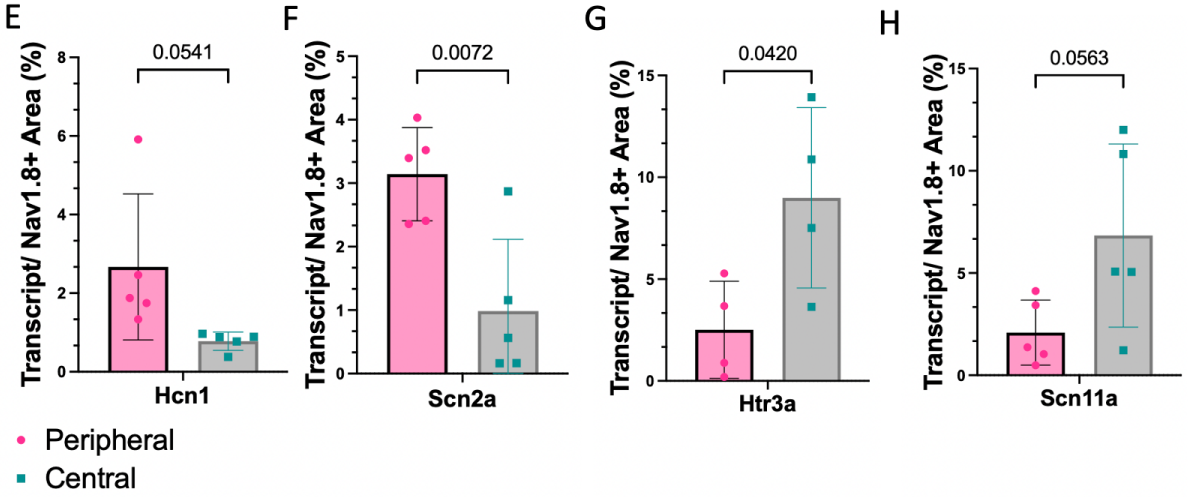
E
F
G
H
Transcript/ Nav1.8+ Area (%)
0.0541
0.0072
0.0420
0.0563
Hcn1
Scn2a
Htr3a
Scn11a
Peripheral
Central

Figure 6

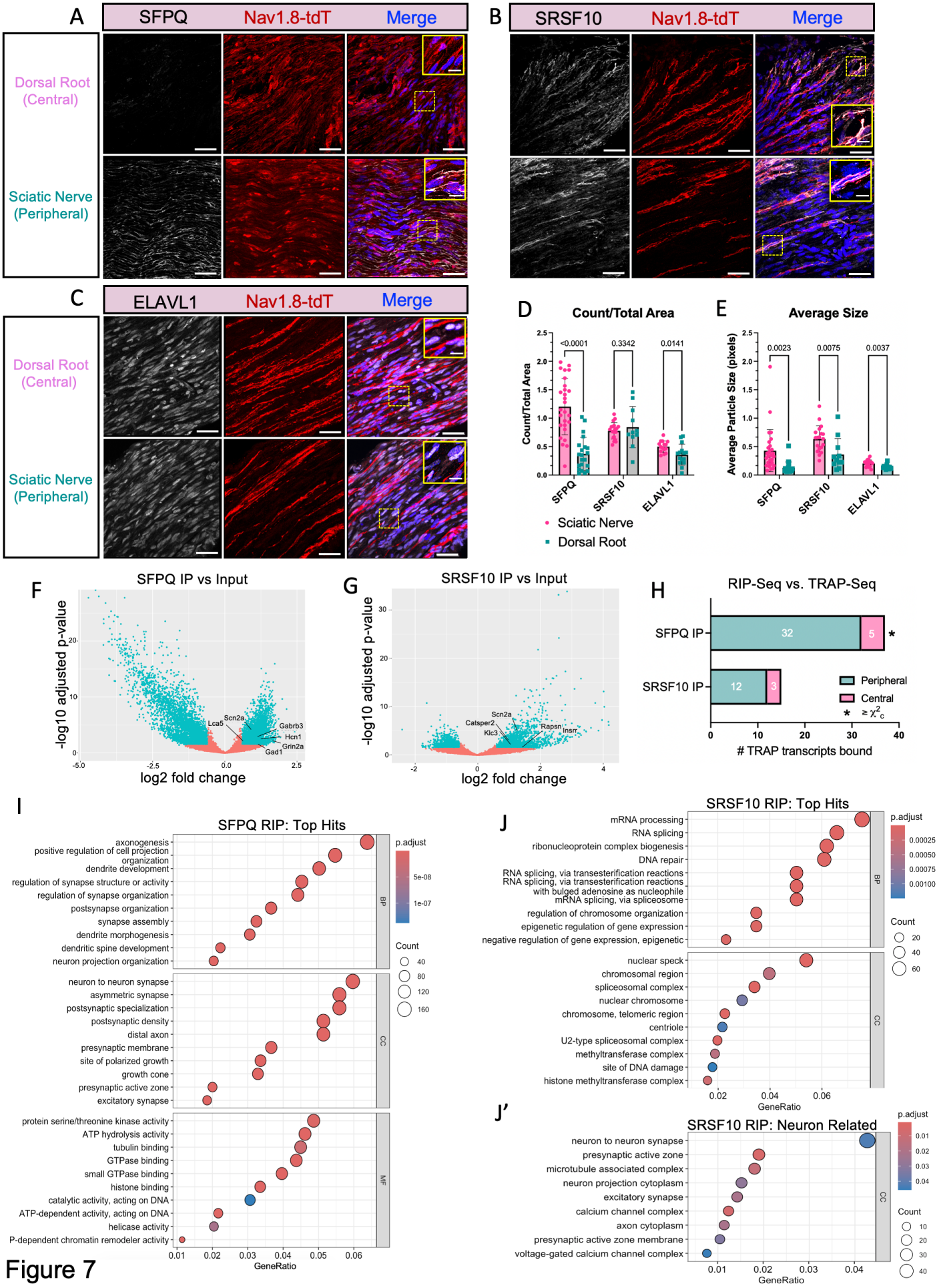
A
SFPQ
Nav1.8-tdT
Merge
Dorsal Root (Central)
Sciatic Nerve (Peripheral)
B
SRSF10
Nav1.8-tdT
Merge
C
ELAVL1
Nav1.8-tdT
Merge
D
Count/Total Area
<0.0001
0.3342
0.0141
Count/Total Area
SFPQ
SRSF10
ELAVL1
Sciatic Nerve
Dorsal Root
E
Average Size
0.0023
0.0075
0.0037
Average Particle Size (pixels)
F
SFPQ IP vs Input
-log10 adjusted p-value
log2 fold change
Lca5
Scn2a
Gabrb3
Hcn1
Grin2a
Gad1
G
SRSF10 IP vs Input
Scn2a
Catsper2
Klc3
Rapsn
Insrr
H
RIP-Seq vs. TRAP-Seq
SFPQ IP
SRSF10 IP
32
5
12
3
Peripheral
Central
TRAP transcripts bound
I
SFPQ RIP: Top Hits
axonogenesis
positive regulation of cell projection organization
dendrite development
regulation of synapse structure or activity
regulation of synapse organization
postsynapse organization
synapse assembly
dendrite morphogenesis
dendritic spine development
neuron projection organization
neuron to neuron synapse
asymmetric synapse
postsynaptic specialization
postsynaptic density
distal axon
presynaptic membrane
site of polarized growth
growth cone
presynaptic active zone
excitatory synapse
protein serine/threonine kinase activity
ATP hydrolysis activity
tubulin binding
GTPase binding
small GTPase binding
histone binding
catalytic activity, acting on DNA
ATP-dependent activity, acting on DNA
helicase activity
P-dependent chromatin remodeler activity
BP
CC
MF
p.adjust
Count
GeneRatio
J
SRSF10 RIP: Top Hits
mRNA processing
RNA splicing
ribonucleoprotein complex biogenesis
DNA repair
RNA splicing, via transesterification reactions
RNA splicing, via transesterification reactions with bulged adenosine as nucleophile
mRNA splicing, via spliceosome
regulation of chromosome organization
epigenetic regulation of gene expression
negative regulation of gene expression, epigenetic
nuclear speck
chromosomal region
spliceosomal complex
nuclear chromosome
chromosome, telomeric region
centriole
U2-type spliceosomal complex
methyltransferase complex
site of DNA damage
histone methyltransferase complex
J'
SRSF10 RIP: Neuron Related
neuron to neuron synapse
presynaptic active zone
microtubule associated complex
neuron projection cytoplasm
excitatory synapse
calcium channel complex
axon cytoplasm
presynaptic active zone membrane
voltage-gated calcium channel complex

Figure 7

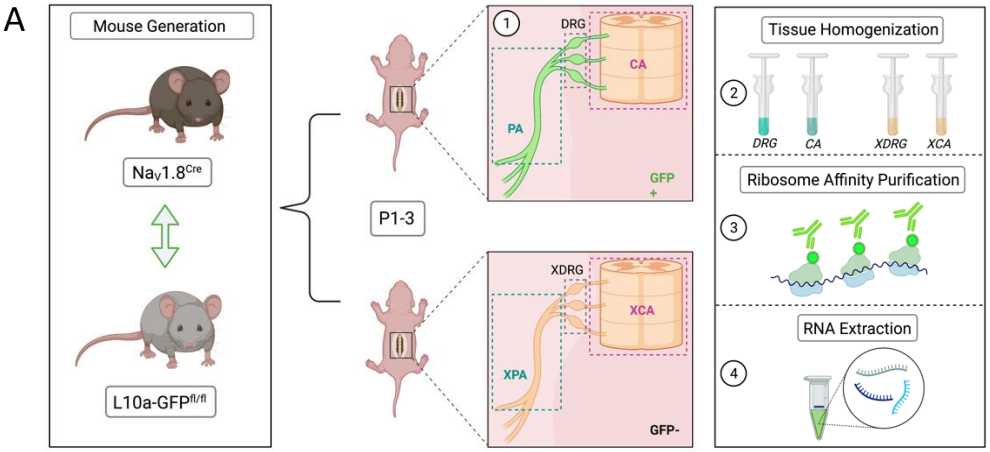
A
Mouse Generation
Nav1.8Cre
L10a-GFPfl/fl
P1-3
1
DRG
CA
PA
GFP +
XDRG
XCA
XPA
GFP-
Tissue Homogenization
2
DRG
CA
XDRG
XCA
Ribosome Affinity Purification
3
RNA Extraction
4

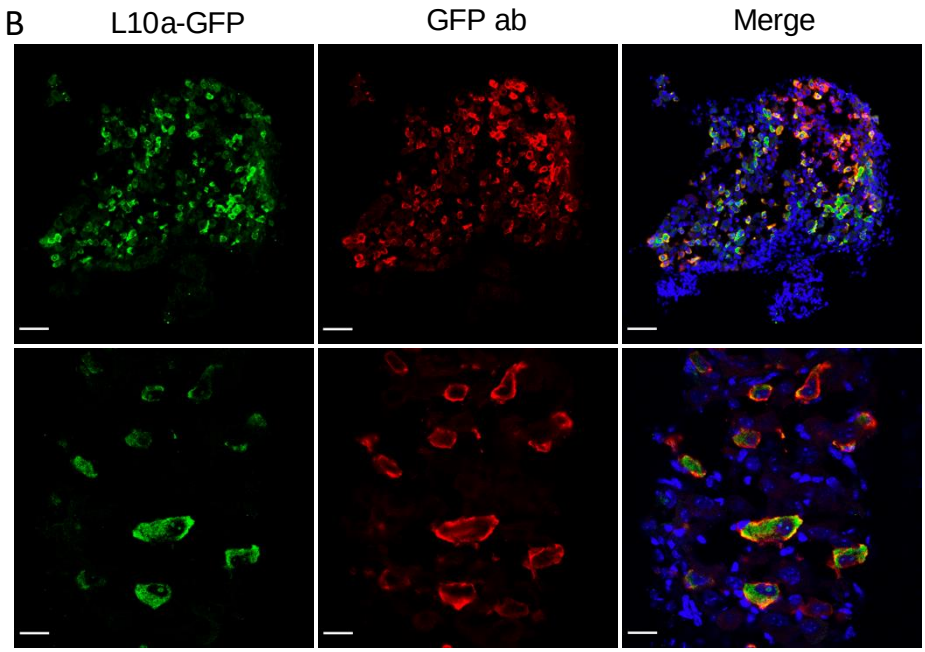
B
L10a-GFP
GFP ab
Merge

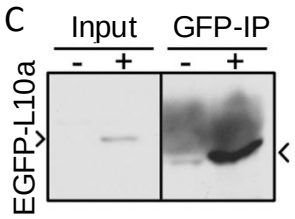
C
Input
GFP-IP
-
+
-
+
EGFP-L10a

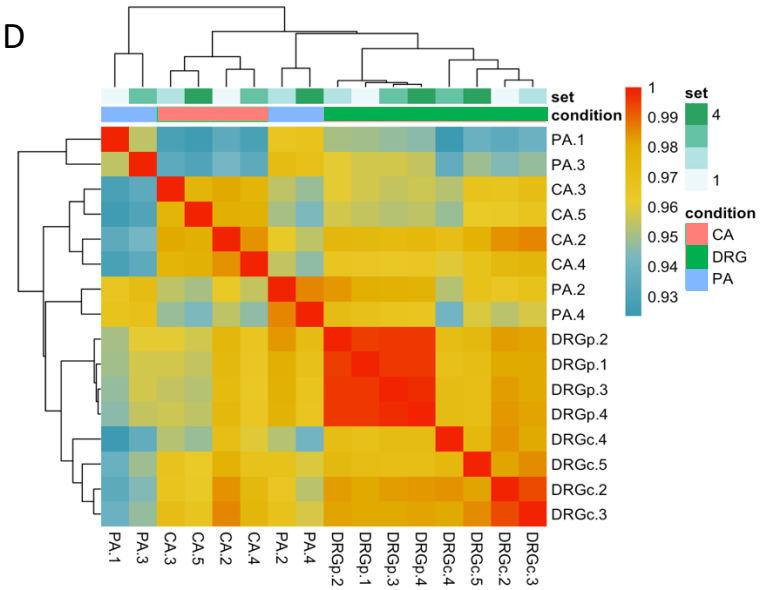
D
set
condition
PA.1
PA.3
CA.3
CA.5
CA.2
CA.4
PA.2
PA.4
DRGp.2
DRGp.1
DRGp.3
DRGp.4
DRGc.4
DRGc.5
DRGc.2
DRGc.3
1
0.99
0.98
0.97
0.96
0.95
0.94
0.93
set
4
1
condition
CA
DRG
PA

Figure S1

Locally Translated Ribosomal Proteins in Peripheral Axon

A

40s Ribosome	Protein Name	Depth[1]	Assembly[2]	CUIC Motif[1]	Observed?[3]
Rps15a	S15a (S8p)	Intermediate	Late-nucleolar	Yes	-
60s Ribosome					
Rpl7	L7/uL30	Surface	Early-nucleolar	No	Yes[1] (xRGC)
Ribosomal-ubiquitin Fusion Proteins					
Rps30/ Fau	S30/ Fubi	N/a	Late-nucleolar	Yes	-
Rps27a	S31	Surface	Cytoplasmic	No	-

Depth- [1]Shigeoka et al., Cell Rep, 2019
Assembly- [2]De la Cruz, Annu Rev Biochem, 2016
CUIC Motif- [1]Shigeoka et al., Cell Rep, 2019
Observed- [3]Fusco et al., Nat Comm, 2021

B

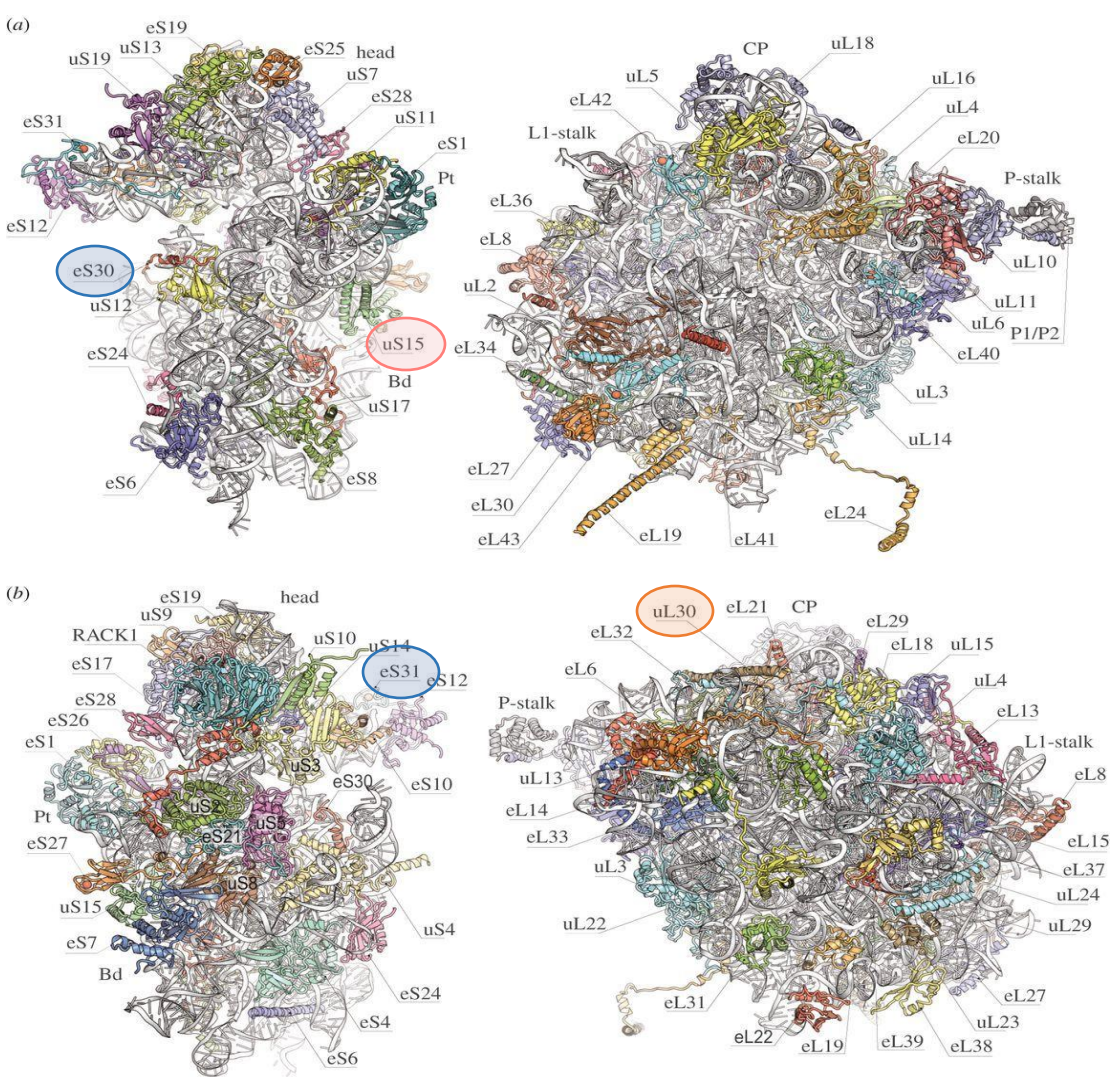

Figure S2

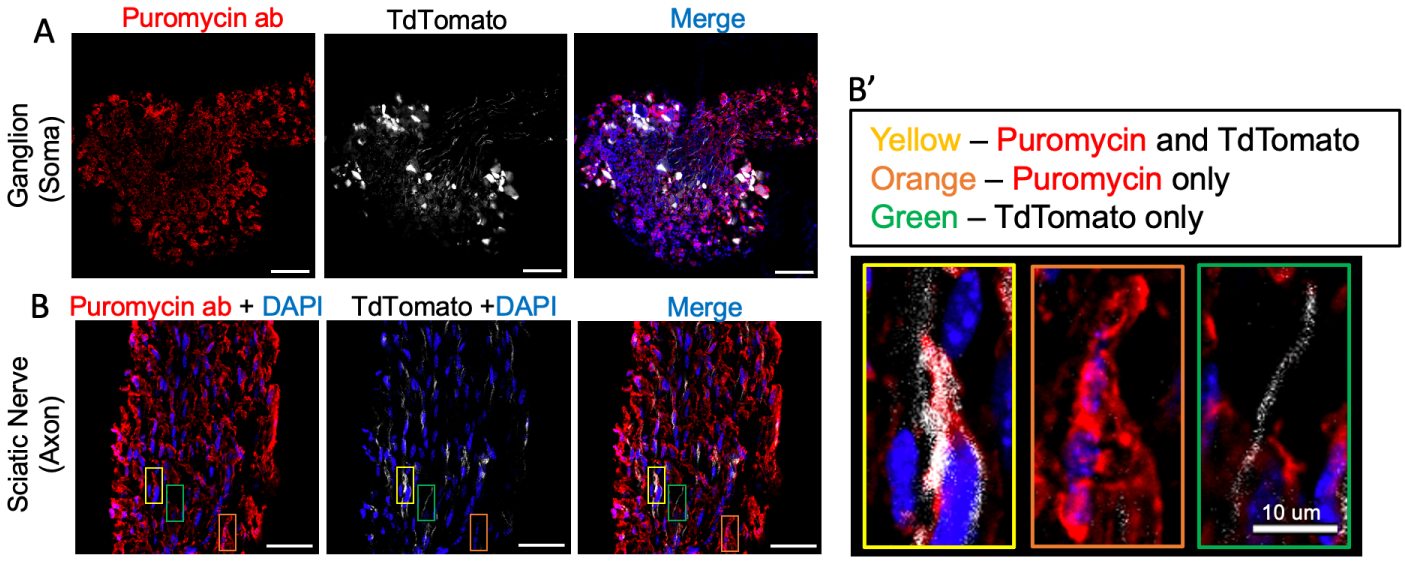
A
Puromycin ab
TdTomato
Merge
Ganglion (Soma)
B
Puromycin ab + DAPI
TdTomato +DAPI
Merge
Sciatic Nerve (Axon)
B'
Yellow – Puromycin and TdTomato
Orange – Puromycin only
Green – TdTomato only
10 um

Figure S3

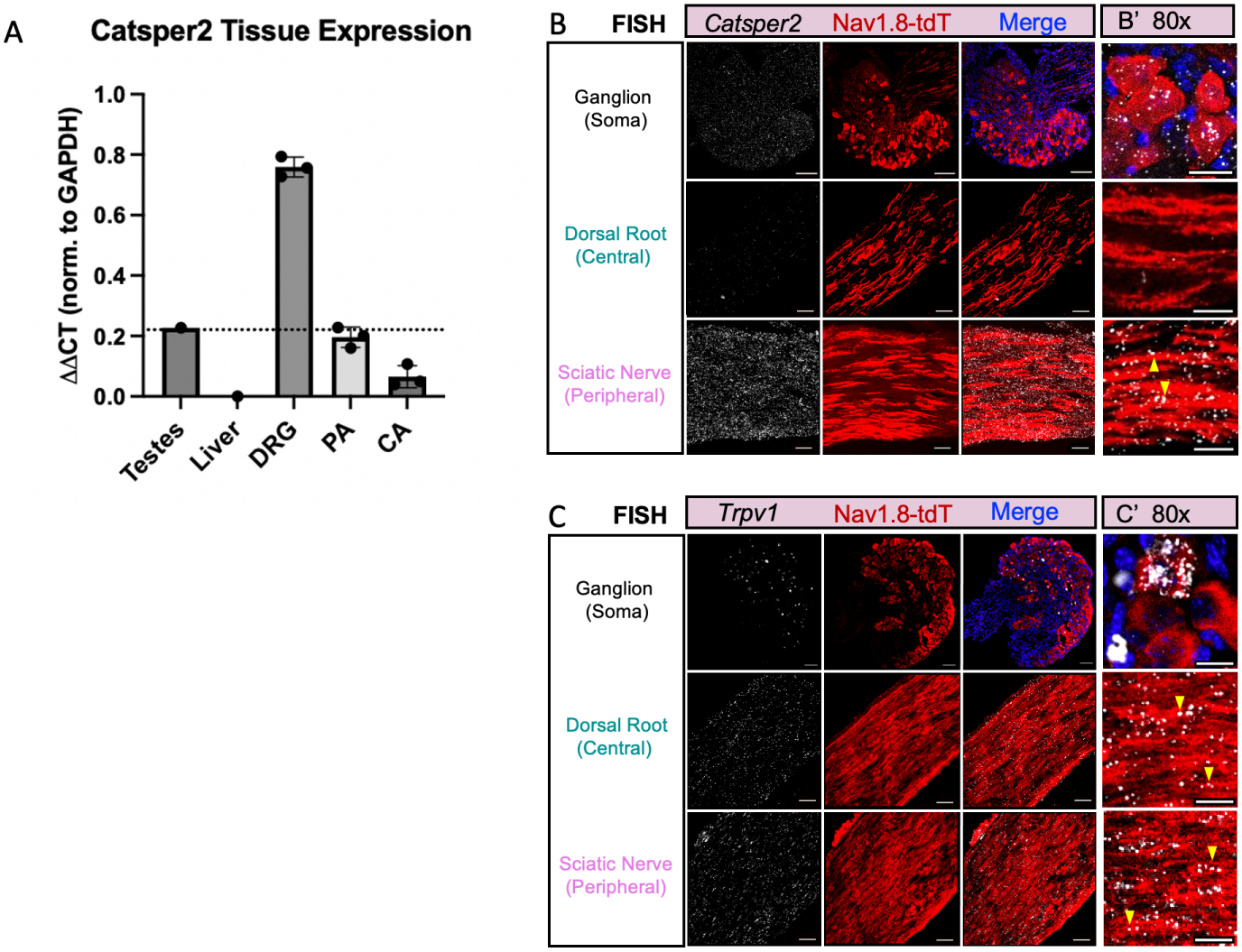
A
Catsper2 Tissue Expression
ΔΔCT (norm. to GAPDH)
1.0
0.8
0.6
0.4
0.2
0.0
Testes
Liver
DRG
PA
CA
B
FISH
Catsper2
Nav1.8-tdT
Merge
B' 80x
Ganglion (Soma)
Dorsal Root (Central)
Sciatic Nerve (Peripheral)
C
FISH
Trpv1
Nav1.8-tdT
Merge
C' 80x
Ganglion (Soma)
Dorsal Root (Central)
Sciatic Nerve (Peripheral)

Figure S4

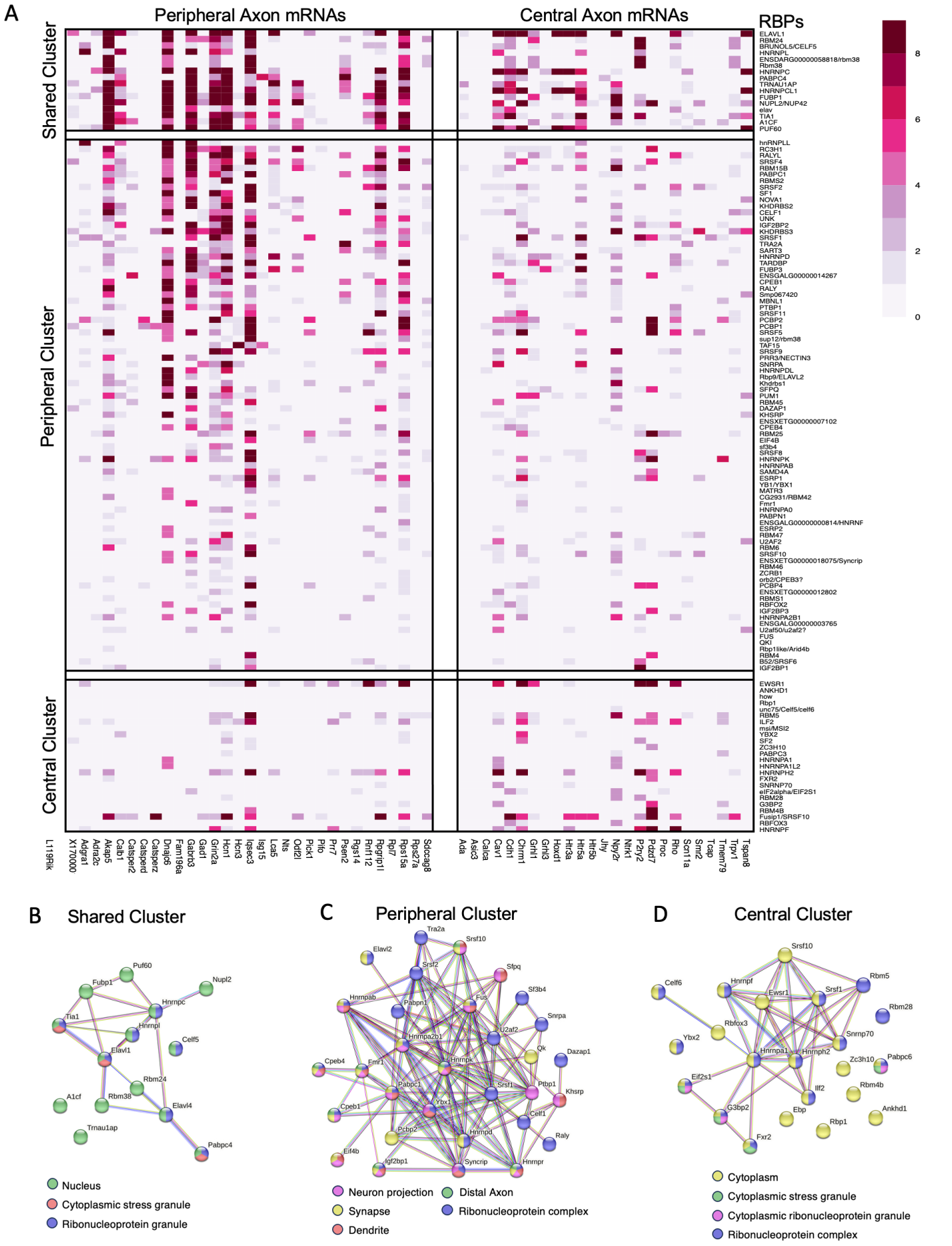
A
Peripheral Axon mRNAs
Central Axon mRNAs
RBPs
Shared Cluster
Peripheral Cluster
Central Cluster
B
Shared Cluster
Nucleus
Cytoplasmic stress granule
Ribonucleoprotein granule
C
Peripheral Cluster
Neuron projection
Distal Axon
Synapse
Ribonucleoprotein complex
Dendrite
D
Central Cluster
Cytoplasm
Cytoplasmic stress granule
Cytoplasmic ribonucleoprotein granule
Ribonucleoprotein complex

Figure S5

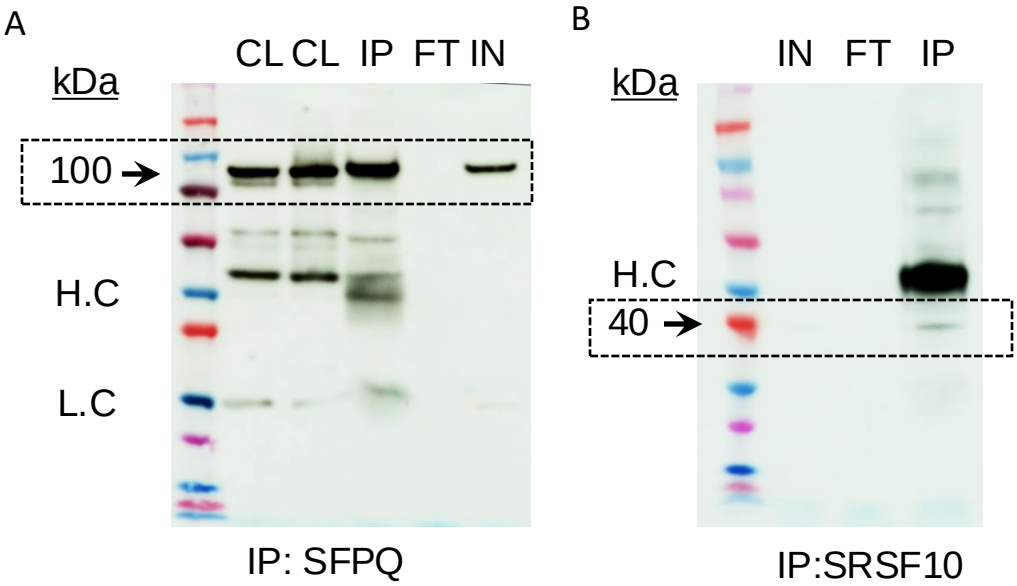

WB sample names:
CL: Positive control lysate
CL: Positive control lysate
IN: Input
FT: Flow-through
IP: Immunoprecipitated

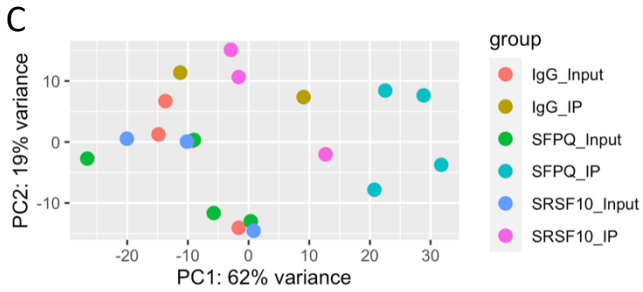

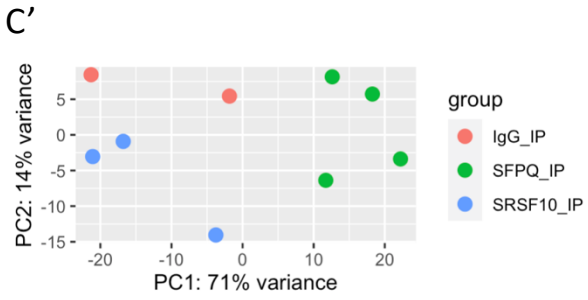

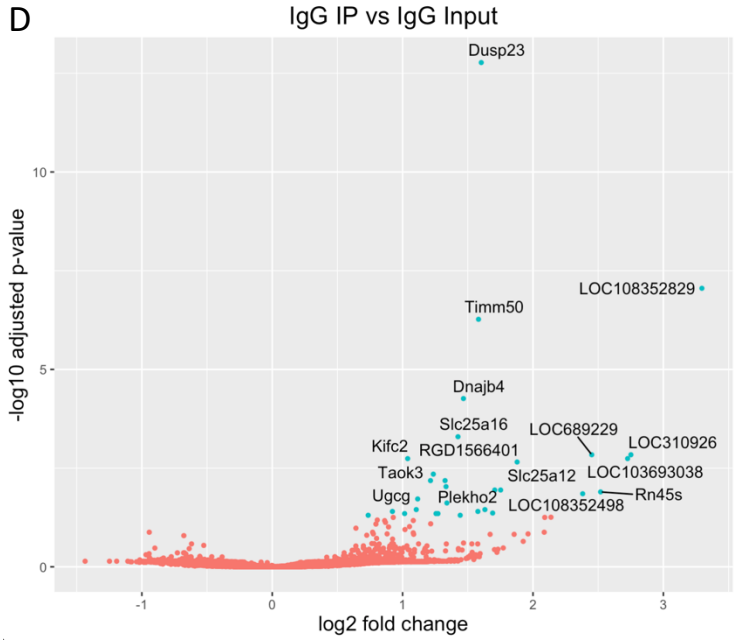

Figure S6

Subcellular
Translating Ribosomal Affinity
Purification (TRAP) Approach

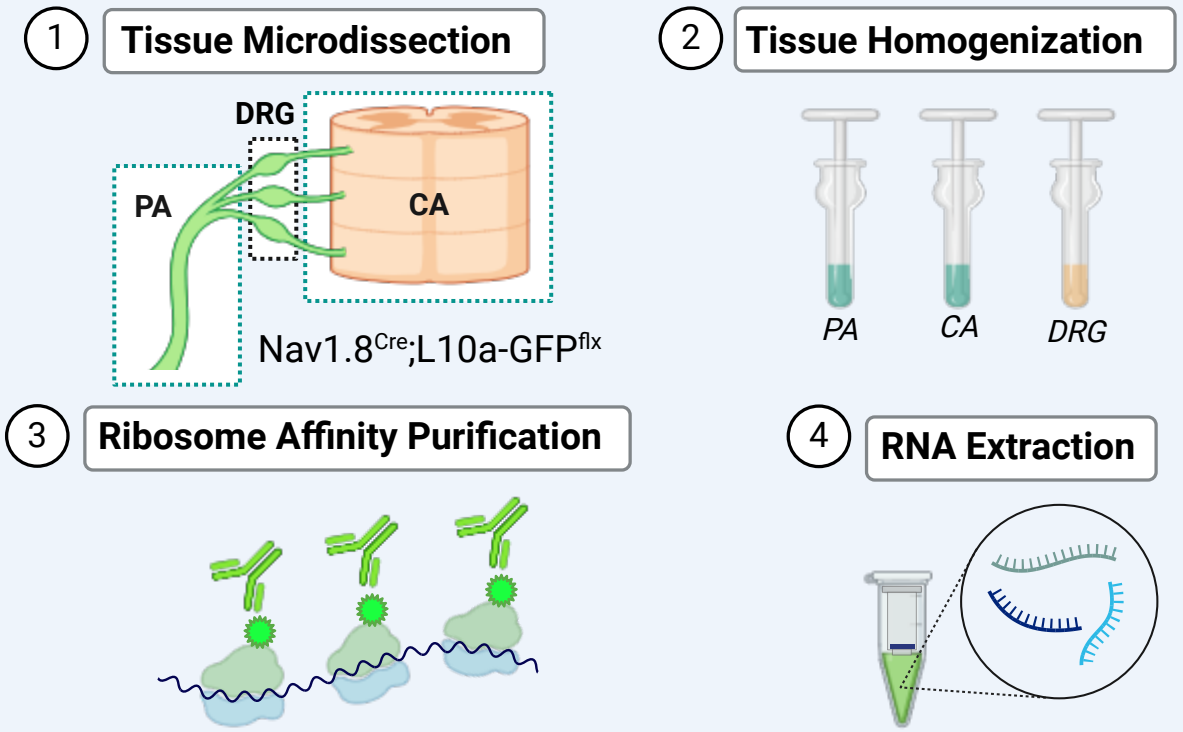

Spatial Translatomes

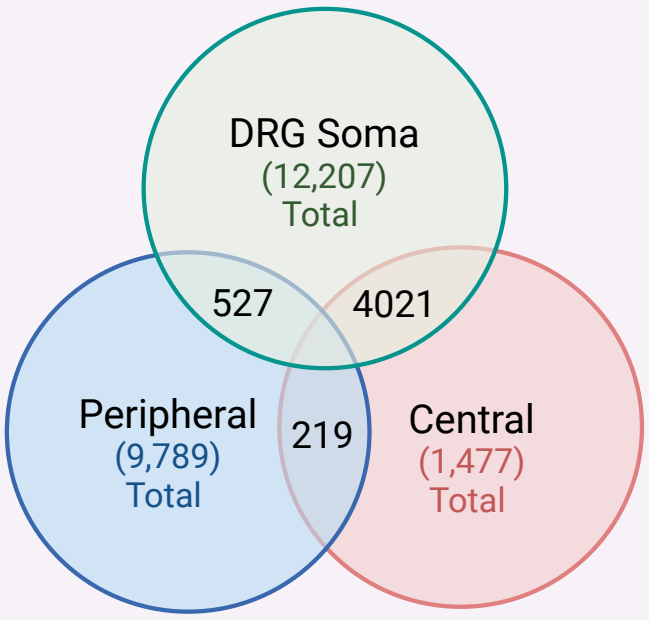

Enriched Biological Processes

Peripheral:
- Neuron projection terminus (*Hcn1/Scn2a*)
- Ciliary basal body
- CatSper complex

Central
- Sensory perception of pain (*Scn11a*)
- Serotonin Binding (*Htr3a*)
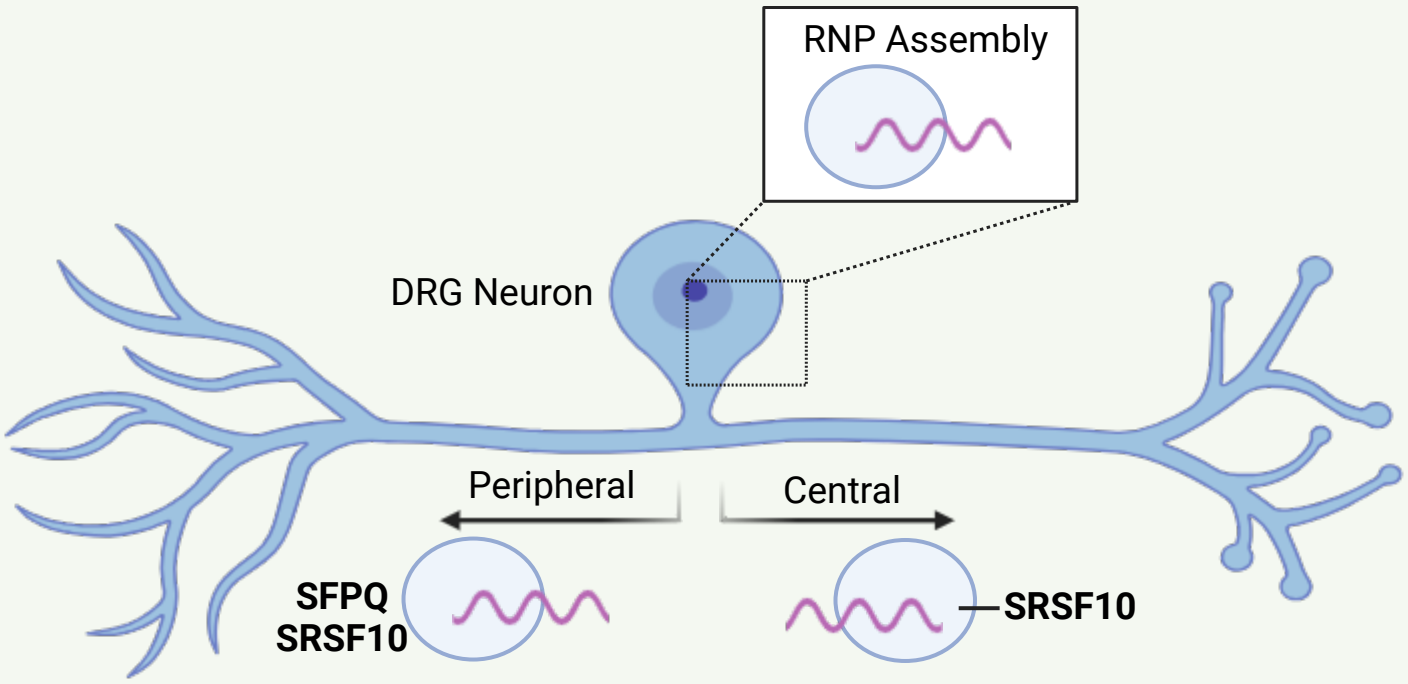
Ribonucleoprotein (RNP)
Granule Sorting